AD_____

Award Number: DAMD17-00-1-0429

TITLE: Radiolabeled Herceptin to Increase Treatment Efficacy in Breast Cancer Patients with Low Tumor HER-2/neu Expression

PRINCIPAL INVESTIGATOR: George Sgouros, Ph.D.

CONTRACTING ORGANIZATION: Sloan-Kettering Institute for Cancer Research
New York, New York 10021

REPORT DATE: July 2003

TYPE OF REPORT: Annual

PREPARED FOR: U.S. Army Medical Research and Materiel Command
Fort Detrick, Maryland 21702-5012

REPORT DOCUMENTATION PAGE

Form Approved
OMB No. 074-0188

1. AGENCY USE ONLY (Leave blank)	2. REPORT DATE	3. REPORT TYPE AND DATES COVERED
	July 2003	Annual (15 Jun 2002 - 14 Jun 2003)

4. TITLE AND SUBTITLE
Radiolabeled Herceptin to Increase Treatment Efficacy in Breast Cancer Patients with Low Tumor HER-2/neu Expression

5. FUNDING NUMBERS
DAMD17-00-1-0429

6. AUTHOR(S)
George Sgouros, Ph.D.

7. PERFORMING ORGANIZATION NAME(S) AND ADDRESS(ES)
Sloan-Kettering Institute for Cancer Research
New York, New York 10021

E-Mail: sgourosg@mskcc.org

8. PERFORMING ORGANIZATION REPORT NUMBER

9. SPONSORING / MONITORING AGENCY NAME(S) AND ADDRESS(ES)
U.S. Army Medical Research and Materiel Command
Fort Detrick, Maryland 21702-5012

10. SPONSORING / MONITORING AGENCY REPORT NUMBER

11. SUPPLEMENTARY NOTES

12a. DISTRIBUTION / AVAILABILITY STATEMENT
Approved for Public Release; Distribution Unlimited

12b. DISTRIBUTION CODE

13. ABSTRACT (Maximum 200 Words)

The primary objective of the proposal is to evaluate the efficacy and feasibility of using radiolabeled Herceptin antibody to target rapidly accessible breast carcinoma cells or micrometastases. By using Herceptin to specifically deliver radiation we anticipate that the efficacy of Herceptin will be extended to include breast cancer cells that are not high HER-2/neu antigen expressors. This hypothesis will be tested using the spheroid model to simulate rapidly accessible micrometastases. An alpha-particle emitting radionuclide will be used to enhance tumor cell kill. Completion of tasks 1-3 and progress towards task 5 was reported in the previous annual report. The animal model previously used towards task 5 was a HER-2/neu expressing ovarian carcinoma. The PI has identified an appropriate disseminated breast carcinoma animal model and will be using this to satisfy the remaining tasks of the proposal. Because the PI relocated in 2003, progress in the past year has been delayed. The PI is in the process of setting up a sub-contract at Hopkins to complete the tasks of the proposal. The sub-contract mechanism is being used because after discussions with the contracting officer this was deemed the most expeditious approach to providing funds for the PI to complete the work at Hopkins

14. SUBJECT TERMS
Herceptin, HER-2/neu, alpha particle emitters, Ac-225, Micrometastases

15. NUMBER OF PAGES
42

16. PRICE CODE

17. SECURITY CLASSIFICATION OF REPORT	18. SECURITY CLASSIFICATION OF THIS PAGE	19. SECURITY CLASSIFICATION OF ABSTRACT	20. LIMITATION OF ABSTRACT
Unclassified	Unclassified	Unclassified	Unlimited

Table of Contents

INTRODUCTION

In combination with chemotherapy, the antitumor activity of Herceptin (anti-Her-2/neu), a humanized monoclonal antibody directed against HER-2/neu, has been effective in treatment of breast cancer cells overexpressing HER-2/neu. This promising, FDA approved, and commercially available antibody may be effective in eradicating pre-vascularized micormetastatic disease when labeled with a short lived alpha particle emitter. Alpha particles are very effective in sterilizing cells, and 1 to 3 particles transversing the cell is enough for cell kill. Therefore, this treatment approach may have the potential of eradicating micrometastatic disease both of non-overexpressing and overexpressing breast cancer cells. These hypotheses will be tested first on a tumor spheroid model that can be closely controlled. Spheroids of breast cancer cells expressing different levels of HER-2/neu will be incubated with Herceptin labeled with an alpha particle emitting radionuclide. This model will be used to determine optimal antibody concentration, dose level and treatment schedule. Using the results obtained from the *in vitro* spheroid system, a pilot effort to obtain preliminary data on treatment response *in vivo* will be undertaken. Spheroids will be injected intraperitoneally in athymic mice and response to Bi-213-Herceptin therapy will be monitored using MR imaging. The cells in the injected spheroids will be tagged with a MRI contrast agent. The potential of Dexamethasone to enhance radiosensitivity by increased apoptotic death will be examined. The proposed study may result in a novel treatment approach where Herceptin will be used to eradicate breast cancer micrometastases expressing HER-2/neu.

In the previous reporting period, Tasks 1-3 were reported complete and progress towards task 5 was presented. Progress in this reporting period has been delayed because the PI has moved and is starting a lab at a different institution. Accordingly the PI is currently arranging for a 1 year no-cost extension for the unexpended $102,193 funds remaining. In response to the review of the previous annual report, the PI has identified a disseminated breast tumor model that will be used to satisfy the animal dose-response tasks, instead of the HER-2/neu expressing ovarian carcinoma used previously as a surrogate for disseminated breast cancer. Details regarding the proposed model and methodologies that will be employed are provided below.

BODY

Task 5 (month 25-26) – Select one cell line and inject spheroids in the peritoneal cavity of mice. Determine baseline growth as measured by MRI

As noted in the previous report, the tumor take following injection of the cell lines listed above was inadequate. We, therefore, moved to an ovarian carcinoma model using a cell line with a high HER-2/neu expression. Using this model we completed microPET imaging of ^{86}Y-Herceptin tumor targeting and also MRI tumor characterization. This work was recently published (1). We have identified a more appropriate model and plan on developing this for accomplishing tasks 6 and 7.

Tasks 6 and 7 (months 27-36) – Use optimal Herceptin concentration and Bi-213 activity as determined in the spheroid model and treat spheroids injected intraperitoneally in mice. Follow response by MRI. Treat animals inoculated with spheroids with Herceptin-Bi-213 in combination with DEX to determine if DEX enhances radiosensitivity. Follow response by MRI.

As noted in an earlier report, Bi-213, initially proposed for use in these studies has become unavailable and was replaced with ^{225}Ac

In response to the reviewer's comments on the previous annual report, a metastatic breast cancer model will be used to complete the tasks of the project. Work will be completed at Johns Hopkins University, School of Medicine under a sub-contract from Memorial Sloan-Kettering Cancer Center which will retain the grant under a "caretaker" PI. This approach was chosen after consultation with the contracting officer as being the most expeditious approach to providing the funds for completion of the project. The model that will be used at Hopkins is described below.

Treatment efficacy will be evaluated in a mouse model of human metastatic breast cancer using cells that have been selected, *in vivo*, to have a high metastatic potential for the skeleton (2). Generation of such cells requires sequential inoculation, collection and expansion of the cells. IP injection of a Ket/Xyl solution will be used to anesthetize the mice for tumor inoculation. Innoculation will be perfomed by injection of 10^5 HER2-expressing MDA-MB-361 tumor cells in a 0.1 ml volume into the left ventricle of the heart using a 30-gauge needle on a tuberculin syringe, inserted percutaneously in the second intercostal space 2 mm to the left of the sternum and aimed centrally. The procedure is associated with a 10 to 14 % mortality rate (2;3). Mice showing evidence of pain or distress will be euthanised by CO_2 inhalation. Development of bone metastases will be monitored radiographically. When the bone mets. reach approx. 2 mm in size (in 4 to 6 weeks). The animals will be sacrificed for bone lesion dissection and expansion of the clonal populations. (Mice showing signs of distress will be euthanized.) To generate a highly metastatic sub-clone (MDA-361-B) clonally expanded cells will be re-innoculated and the metastatic cells collected for expansion 2 more times.

Groups of 15 mice will be injected with the MDA-361-B cell line after it has been transfected with the firefly luciferase gene for bioluminescent imaging (2;4). Cells will be transfected with a CMV promoter-driven mammalian expression vector for luciferase (phRL-CMV; Promega, Corp., Cat # E6271) using a liposomal transfection method (fugene-6; Roche Applied Diag., Cat No. 181442); stable transfectants will be selected using G418 (Clonetech, Cat # 8056). At 25 days bioluminescent imaging will be performed. Animals will be IP-injected with 30 µl of a 250 mM solution of luciferin (Molecular Probes, Cat # L-2912) 15 min. prior to imaging. After 5 minutes of photon collection and verification that disseminated disease exists, the mice will be injected by dorsal tail vein with ^{225}Ac-Herceptin. .

KEY RESEARCH ACCOMPLISHMENTS (prior and current reporting period)

- Generated and characterized the growth of spheroids expressing different levels of HER-2/neu receptor.
- Evaluated the radiosensitivities of the three cell lines used for generating the spheroids.
- Characterized antibody penetration kinetics into HER-2/neu expressing spheroids.
- Evaluated the response of HER-2/neu expressing spheroids to Herceptin and to Ac-225 labeled antibody
- Demonstrated of the feasibility of controlling tumor cell clusters with intermediate expression of HER-2/neu using Ac-225-labeled Herceptin
- Demonstrated microPET imaging of HER-2/neu expressing tumor and MRI-based size determinations
- Identified appropriate disseminated breast cancer model for therapeutic studies

REPORTABLE OUTCOMES

Published paper: Palm S, Enmon RM, Matei C, Kolbert KS, Xu S, Pellegrini V, Zanzonico PB, Finn RL, Koutcher JA, Larson SM, Sgouros G. Pharmacokinetics and biodistribution of ^{86}Y-Trastuzumab for ^{90}Y dosimetry in an ovarian carcinoma model: Correlative microPET and MRI. J Nucl Med 2003;44:1148-1155.

Manuscript, in preparation: Ballangrud AM, Yang W-H, Palm S, Enmon R, Borchardt PE, Pellegrini VA, McDevitt MR, Scheinberg DA, Sgouros G. Alpha-particle emitting atomic generator (Ac225)-labeled Herceptin targeting breast cancer spheroids: efficacy versus HER-2/neu expression

CONCLUSIONS

Tasks 1-3 have been completed, Preliminary work towards task 5 has been published but will be repeated using a more appropriate, breast-cancer specific model. Remaining tasks will be completed at Johns Hopkins Univeristy, School of Medicine.

Dose-response results obtained with MDA MB361 spheroids suggest that it will be possible to eradicate tumor cells with intermediate expression of HER-2/neu using Ac-225-labeled herceptin at a concentration between 100 and 500 nCi/ml. Scaled up to human administration, assuming an initial distribution volume of 3L (i.e., the plasma volume), this activity concentration translates to approximately a 1 mCi injection of ^{225}Ac-Herceptin. Based on animal studies, this activity concentration is clinically realistic (*9*).

SO WHAT? These preliminary studies suggest that by using Herceptin antibody radiolabeled with an alpha-particle emitter it may be possible to treat breast cancer patients whose tumor does not demonstrate high expression of HER-2/neu.

Reference List

1. Palm,S., Enmon,R.M., Jr., Matei,C., Kolbert,K.S., Xu,S., Zanzonico,P.B., Finn,R.L., Koutcher,J.A., Larson,S.M., and Sgouros,G. 2003. Pharmacokinetics and Biodistribution of (86)Y-Trastuzumab for (90)Y Dosimetry in an Ovarian Carcinoma Model: Correlative MicroPET and MRI. *J Nucl Med* 44:1148-1155.

2. Wetterwald,A., van der,P.G., Que,I., Sijmons,B., Buijs,J., Karperien,M., Lowik,C.W., Gautschi,E., Thalmann,G.N., and Cecchini,M.G. 2002. Optical imaging of cancer metastasis to bone marrow: a mouse model of minimal residual disease. *Am.J Pathol.* 160:1143-1153.

3. Arguello,F., Baggs,R.B., and Frantz,C.N. 1988. A murine model of experimental metastasis to bone and bone marrow. *Cancer Res.* 48:6876-6881.

4. Stensrud,G., Redford,K., Smistad,G., and Karlsen,J. 1999. Effects of gamma irradiation on solid and lyophilised phospholipids. *Rad Phys Chem* 56:611-622.

Appendix Material

1. Palm,S., Enmon,R.M., Jr., Matei,C., Kolbert,K.S., Xu,S., Zanzonico,P.B., Finn,R.L., Koutcher,J.A., Larson,S.M., and Sgouros,G. 2003. Pharmacokinetics and Biodistribution of (86)Y-Trastuzumab for (90)Y Dosimetry in an Ovarian Carcinoma Model: Correlative MicroPET and MRI. *J Nucl Med* 44:1148-1155.

2. Ballangrud AM, Yang W-H, Palm S, Enmon R, Borchardt PE, Pellegrini VA, McDevitt MR, Scheinberg DA, Sgouros G. Alpha-particle emitting atomic generator (Ac225)-labeled Herceptin targeting breast cancer spheroids: efficacy versus HER-2/neu expression

Pharmacokinetics and Biodistribution of ^{86}Y-Trastuzumab for ^{90}Y Dosimetry in an Ovarian Carcinoma Model: Correlative MicroPET and MRI

Stig Palm, PhD[1]; Richard M. Enmon, Jr., PhD[1]; Cornelia Matei, SB[1]; Katherine S. Kolbert, MS[1]; Su Xu, PhD[1]; Pat B. Zanzonico, PhD[1]; Ronald L. Finn, PhD[1]; Jason A. Koutcher, MD, PhD[1]; Steven M. Larson, MD[2]; and George Sgouros, PhD[1,3]

[1]Department of Medical Physics, Memorial Sloan-Kettering Cancer Center, New York, New York; [2]Department of Radiology, Memorial Sloan-Kettering Cancer Center, New York, New York; and [3]Department of Radiology, Johns Hopkins University School of Medicine, Baltimore, Maryland

Preclinical biodistribution and pharmacokinetics of investigational radiopharmaceuticals are typically obtained by longitudinal animal studies. These have required the sacrifice of multiple animals at each time point. Advances in small-animal imaging have made it possible to evaluate the biodistribution of radiopharmaceuticals across time in individual animals, in vivo. MicroPET and MRI-based preclinical biodistribution and localization data were obtained and used to assess the therapeutic potential of ^{90}Y-trastuzumab monoclonal antibody (mAb) (anti-HER2/neu) against ovarian carcinoma. **Methods:** Female nude mice were inoculated intraperitoneally with $5 \cdot 10^6$ ovarian carcinoma cells (SKOV3). Fourteen days after inoculation, 12–18 MBq ^{86}Y-labeled trastuzumab mAb was injected intraperitoneally. Tumor-free mice, injected with ^{86}Y-trastuzumab, and tumor-bearing mice injected with labeled, irrelevant mAb or ^{86}Y-trastuzumab + 100-fold excess unlabeled trastuzumab were used as controls. Eight microPET studies per animal were collected over 72 h. Standard and background images were collected for calibration. MicroPET images were registered with MR images acquired on a 1.5-T whole-body MR scanner. For selected time points, 4.7-T small-animal MR images were also obtained. Images were analyzed and registered using software developed in-house. At completion of imaging, suspected tumor lesions were dissected for histopathologic confirmation. Blood, excised normal organs, and tumor nodules were measured by γ-counting. Tissue uptake was expressed relative to the blood concentration (percentage of injected activity per gram of tissue [%IA/g]/%IA/g blood). ^{86}Y-Trastuzumab pharmacokinetics were used to perform ^{90}Y-trastuzumab dosimetry. **Results:** Intraperitoneal injection of mAb led to rapid blood-pool uptake (5–9 h) followed by tumor localization (26–32 h), as confirmed by registered MR images. Tumor uptake was greatest for ^{86}Y-trastuzumab (7 ± 1); excess unlabeled trastuzumab yielded a 70% reduction. Tumor uptake for the irrelevant mAb was 0.4 ± 0.1. The concentration in normal organs relative to blood ranged from 0 to 1.4 across all studies, with maximum uptake in spleen. The absorbed dose to the kidneys was 0.31 Gy/MBq ^{90}Y-trastuzumab. The liver received 0.48 Gy/MBq, and the spleen received 0.56 Gy/MBq. Absorbed dose to tumors varied from 0.10 Gy/MBq for radius = 0.1 mm to 3.7 Gy/MBq for radius = 5 mm. **Conclusion:** For all injected compounds, the relative microPET image intensity of the tumor matched the subsequently determined ^{86}Y uptake. Coregistration with MR images confirmed the position of ^{86}Y uptake relative to various organs. Radiolabeled trastuzumab mAb was shown to localize to sites of disease with minimal normal organ uptake. Dosimetry calculations showed a strong dependence on tumor size. These results demonstrate the usefulness of combined microPET and MRI for the evaluation of novel therapeutics.

Key Words: microPET; trastuzumab; ^{86}Y; ovarian carcinoma; pharmacokinetics

J Nucl Med 2003; 44:1148–1155

Pharmacokinetics and biodistribution of radiopharmaceuticals in preclinical animal studies have generally been obtained by extraction of selected organs and scintillation counting for radioactivity at different times after injection. This approach requires the sacrifice of multiple animals at each time point, precludes the ability to monitor biodistribution in individual animals, and is partially susceptible to selection bias because unexpected accumulation of radioactivity in tissue not collected for scintillation counting will be missed. The availability of small-animal imaging instrumentation and positron-emitting analogs of therapeutic radionuclides (e.g., ^{86}Y and ^{124}I for ^{90}Y and ^{131}I, respectively) has made it possible to obtain preclinical pharmacokinetics noninvasively using imaging-based methods. The advantages of such an approach include the ability to monitor kinetics in individual animals over time and the ability to

Received Nov. 5, 2002; revision accepted Mar. 24, 2003.

For correspondence or reprints contact: Stig Palm, PhD, Department of Medical Physics, Memorial Sloan-Kettering Cancer Center, 1275 York Ave., New York, NY 10021.

E-mail: palms@mskcc.org

obtain whole-body images of biodistribution, thereby reducing the likelihood that areas of unexpected radiopharmaceutical accumulation will be missed. Together, these increase the statistical power of each measurement, reducing total animal requirements. The disadvantages include a reduction in quantitative accuracy and difficulty in placing the radioactivity distribution in the proper anatomic context. The latter difficulty arises because of resolution limitations and because images of radionuclide distribution do not typically provide detailed anatomic information.

In this work, the positron-emitting radionuclide ^{86}Y, in conjunction with small-animal PET (microPET) imaging, is used to evaluate pharmacokinetics and dosimetry of ^{90}Y-trastuzumab in a disseminated ovarian carcinoma model. MRI, in conjunction with image registration, was used to correlate the radiolabeled monoclonal antibody (mAb) distribution with anatomy. At the end of imaging, the animals were killed and conventional organ biodistribution information was obtained by γ-counting. The combination of these approaches satisfactorily addressed the issues of anatomic localization and quantitative accuracy.

^{86}Y has a 14.7-h half-life ($t_{1/2}$) and decays by positron emission. The relatively long half-life allows the acquisition of PET images 2–3 d after injection. Being isotopes of the same element, ^{86}Y is chemically identical to ^{90}Y, a pure β-particle–emitting radionuclide that is under investigation for use in targeted radionuclide therapy (*1,2*). A drawback of using ^{90}Y is that the lack of emitted photons makes it difficult to study the biodistribution of the injected compound. To overcome this obstacle, alternative nuclides have been used. The most commonly used is ^{111}In; however, with PET cameras becoming more available, the use of the positron emitter ^{86}Y has been suggested as a better substitute. A nuclide of the same element is expected to behave chemically identically and thus serve better than a nuclide of another element. Comparisons between these 2 ^{90}Y substitutes—that is, ^{111}In and ^{86}Y—have recently been made (*3,4*).

The anti-HER2/neu mAb, trastuzumab, has demonstrated efficacy in the treatment of cancer patients whose disease exhibits high levels of HER2/neu expression (*5,6*). In several studies, trastuzumab has been shown to potentiate chemotherapy (*7,8*). The possibility of using radiolabeled anti-HER2/neu mAbs for cancer therapy has been previously considered (*9*).

MATERIALS AND METHODS

Cell Culture and Tumor Inoculation

The human ovarian carcinoma cell line SKOV3-NMP2 was provided by Dr. Paul Borchardt (Memorial Sloan-Kettering Cancer Center [MSKCC]). Subclone NMP2 was originally created at the University of Texas M.D. Anderson Cancer Center by passage of the line through nude mice and selected for this study because of enhanced tumorigenicity (*10*). Stock T-flask cultures were propagated at 37°C, in 95% relative humidity, and in 5% CO_2 in RPMI 1640 medium (Invitrogen) supplemented with 10% fetal calf serum (Sigma), 100 units/mL penicillin, and 100 mg/mL streptomycin (Gemini Bio-Products). Cell concentrations were determined by counting trypsinized cells with a hemocytometer. Tumor inoculum was prepared as a single-cell suspension at $1 \cdot 10^7$ cells/mL in complete RPMI 1640 medium. Each 4- to 6-wk-old female BALB/c nude mouse (Taconic) received 0.5 mL inoculum ($5 \cdot 10^6$ cells) administered by intraperitoneal injection. Animals receiving 0.5 mL of media alone served as negative controls.

Mice were housed in filter top cages and provided with sterile food and water. Animals were maintained according to the regulations of the Research Animal Resource Center at MSKCC, and animal protocols were approved by the Institutional Animal Care and Use Committee.

Preparation of Radioimmunoconjugate

mAb–chelate conjugates were provided as gifts: humanized anti-HER-2, trastuzumab (Herceptin; Genentech, Inc.), was provided by Dr. Paul Borchardt and prepared according to Borchardt et al. (*11*); humanized anti-CD33, HuM195 (Protein Design Labs, Inc.), was provided by Dr. Michael McDevitt (MSKCC) and prepared according to McDevitt et al. (*12*). A backbone-substituted derivative of diethylenetriamine pentaacetic acid (DTPA), 2-(4-isothiocyanatobenzyl)DTPA (SCN-CHX-A-DTPA), served as the chelate in all conjugation reactions. mAb conjugate was typically supplied at 7–10 mg/mL.

^{86}Y was produced by irradiating isotope-enriched $^{86}SrCO_3$ (97.02% ^{86}Sr) with 15-MeV protons in the cyclotron facility (model CS-15; Cyclotron Corp.) of MSKCC (*13*). The ^{86}Y was dissolved in 0.2–0.4 mL of 50 mmol/L HCl, generating $^{86}YCl_3$. The radioactivity was measured with a dose calibrator (model CRC-15R; Capintec) and a NaI(Tl) γ-counter (model 5003, Cobra II; Packard).

Radiolabeling protocols were based on those developed in Nikula et al. (*14,15*). These references similarly outline methods for assessing reaction efficiency using instant thin-layer chromatography (ITLC) and for evaluating final immunoreactivity of the product. Briefly, 0.2–0.3 mL of 3 mol/L ammonium acetate was added to the $^{86}YCl_3$ solution to adjust to pH ~5.5. Approximately 200 μg of mAb conjugate were added and the reaction was allowed to proceed at 25°C for 30 min. The reaction was quenched by the addition of 0.040 mL of 10 mmol/L ethylenediaminetetraacetic acid. Radiolabeled mAb was purified from unbound isotope by size-exclusion chromatography using a 10-DG size-exclusion column (Bio-Rad Laboratories, Inc.). Minimum reaction efficiency was 70% as determined by ITLC. The radioactivity of the eluent was determined as previously described. Specific activity varied from 0.7 to 1.0 MBq/μg. Immunoreactivity as determined by acid wash was >90%.

MicroPET Imaging

Two weeks after tumor inoculation, each mouse received 15 MBq (~20 μg) labeled mAb in 0.5 mL RPMI 1640 medium administered intraperitoneally. Mice receiving radiolabeled HuM195 prepared similarly or 15 MBq free ^{86}Y in 0.5 mL medium served as negative controls. A competitive control was created by adding an additional 2 mg unlabeled mAb to the injectate (excess cold control). For each experiment, a 20-mL glass scintillation vial filled with medium and containing 15 MBq ^{86}Y-trastuzumab was used as a standard. The microPET scanner used in these studies was not fitted with a transmission source; therefore, transmission studies were not collected for attenuation correction of the emission data.

Time-dependent distribution and localization of mAb were determined by 8 microPET imaging sessions over the course of 3 d. During each session a background scan and an image of the standard were also acquired. With the exception of the background, a minimum of $15 \cdot 10^6$ true counts per scan were collected to ensure adequate image quality. This required aquisition times of 2–5 min on day 0, 10–20 min on day 1, and 40 min on day 2 or 3 after injection. The mice were initially anesthetized using an isoflurane (Forane; Baxter) loaded vaporizer (Vetequip) attached to an incubation chamber. The mice were then placed on the imaging table and were kept anesthetized during the image acquisition by switching the vaporizer to a fitted nose cone.

MRI

On day 5 or 6 after injection, each mouse was imaged on a 1.5-T whole-body MR scanner (Signa; General Electric Medical Systems) to provide anatomic images for registration with PET scans. Five or 6 mice were anesthetized using 106 mg/kg ketamine and 5.5 mg/kg acepromasine, placed in an in-house–fabricated mouse coil designed for imaging up to 13 mice simultaneously (*16*), and imaged in a single 30- to 40-min session. Imaging parameters included a field of view of 8 × 8 mm, slice thickness of 1.5 mm, slice interval of 0.5 mm, imaging matrix of 512 × 512, a fast spin echo pulse sequence with a repetition interval (TR) of 4,500–11,000 ms, echo time (TE) arranged 96–102 ms, and 4 excitations per phase-encoding step. Selected mice were further imaged on a small-animal 4.7-T MR scanner (Omega; General Electric Medical Systems). A T2-weighted pulse sequence was also used on the 4.7-T scanner with a TR of 3,500 ms, TE of 40 ms, 1-mm-thick slice, imaging matrix of 256 × 256, and a 3-cm field of view.

Image Analysis and MicroPET Activity Quantitation

Image reconstruction was performed by filtered backprojection. In-house–developed software, MIAU (*17*) and 3-dimensional internal dosimetry (3D-ID) package (*18*), were used to quantitate reconstructed images and also for registration to MR studies. Whole-body clearance kinetics were obtained from the summed counts in each scan at each time point. Total counts were corrected for dead time and background. The decay-corrected total counts for the standard obtained in this manner varied by <2% over 72 h. Relative activity concentrations over the injection site, heart, and tumor were obtained by drawing regions of interests (ROIs). MicroPET quantitation can be influenced by the position of tissue relative to the central axis of the camera and also by the surrounding tissue, due to differential sensitivity and attenuation, respectively. Direct comparison of tumor to organ activity concentration was therefore not made; rather, only relative changes in the activity concentration in these tissues over time were evaluated. To minimize partial-volume effects arising because the activity containing volume (e.g., tumor nodules) is below the intrinsic resolution of the scanner, ROIs were consistently drawn to enclose a 30- to 40-μL volume.

Excised Organ Quantitation

Mice were killed on day 6 after injection by CO_2 intoxication for dissection. Blood was collected via cardiac puncture. Organ, muscle, and tumor tissues were washed in phosphate-buffered saline and weighed. The samples were then counted for photons in a γ-counter (model 5003, Cobra II; Packard). Two 100-μL aliquots of the 20-mL imaging standard were used for calibration of γ-counting results. Results are expressed as the radioactivity concentration in each organ divided by the concentration in blood.

Dosimetry

^{86}Y-Trastuzumab kinetics and biodistribution were used to estimate absorbed doses for trastuzumab labeled with ^{90}Y, the therapeutically relevant radionuclide. Absorbed doses were estimated for the liver, kidneys, spleen, and tumor. A time–activity curve for blood was generated by determining the relative activity concentration from ROIs over the heart on repeated microPET images. The curve was then scaled to fit the activity concentration in collected blood at the time of dissection by extrapolating the monoexponential clearance phase of the curve. The activity concentration in liver, spleen, and kidneys was determined by γ-counting after dissection. The shape of the blood time–activity curve was used to construct a time–activity curve for each organ. The curve was scaled so that the activity concentration of the curve yielded the measured concentration at the time of dissection.

Tumor kinetics were obtained using the tumor ROI. Activity concentration in dissected tumor was fit to an extrapolated plateau in the time–activity curve. All curves were converted to represent physical-decay–corrected ^{86}Y-trastuzumab uptake (% injected activity per gram tissue, %IA/g). Assuming the same distribution for ^{90}Y-trastuzumab, the cumulated activity concentration ($\tilde{A}$/g) was calculated by integrating the decay-corrected uptake curves with the physical half-life of ^{90}Y:

$$\frac{\tilde{A}}{g} = \int_0^\infty A_0 \cdot \frac{f(t)}{100} \cdot e^{-\lambda \cdot t} dt, \qquad \text{Eq. 1}$$

where A_0 is the total amount of ^{90}Y-trastuzumab activity injected in the mouse (Bq), $f(t)$ is the time-dependent uptake of ^{90}Y-trastuzumab (%IA/g), and λ is the decay constant of ^{90}Y ($3.0038 \cdot 10^{-6}$ s^{-1}).

Absorbed doses were calculated following the MIRD formalism (*19*). Absorbed fractions of electron energy emitted from a homogeneous distribution of ^{90}Y in spheres of various sizes (*20*) were used for tumor absorbed dose calculations. Recently published murine-specific S factors (*21*) were used to calculate self and cross-organ absorbed dose for liver, spleen, and kidneys. In the work cited, murine S factors were generated on the basis of the anatomic structure of an actual mouse as defined by noninvasive, high-resolution MRI. Using the previously developed 3D-ID package (*18*), organ contours were drawn and the resulting 3-dimensional organ volumes were convolved with individual radioisotope point kernels to calculate the S-factor values.

RESULTS

Tumor Take

The efficiency of tumor formation in this ovarian carcinoma model was 100% (n = 23). A consistent tumor distribution pattern was observed with histologically confirmed tumor nodules always appearing within 2–3 wk on the ventral side of the spleen (Fig. 1). Tumor was also frequently found dispersed within the mesentery with small (~1 mm), dense tumor nodules forming a "beads-on-a-string" configuration.

MicroPET Imaging

Time-sequential microPET images of coronal slices selected through the same plane (2 or 3 slices, ~1 mm, above

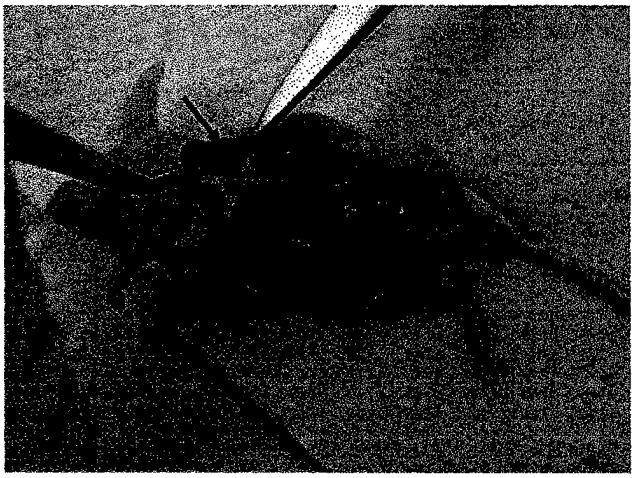

FIGURE 1. Dissected mouse. Arrow indicates location of small tumor nodules on spleen.

the bed) are shown in Figure 2. Images obtained using the specific mAb (n = 8) show high intensity at the injection site and subsequent accumulation of radioactivity in the circulation, as reflected by high cardiac signal intensity. This first becomes visible within 3 h and is most intense at ~20 h after injection. Over this same time course tumor nodules become visible, first in the intestinal area and subsequently (e.g., by 30–40 h after injection) in the vicinity of the spleen. Tumor nodules were consistently visualized around the spleen in all animals. By 71 h, activity in the circulation is reduced and radioactivity persists at histopathologically confirmed tumor sites. In the 71-h image, the localization that is observed near the injection site corresponds to subcutaneous tumor nodules that occur as a result of the intraperitoneal tumor cell inoculation.

Corresponding coronal slices for several different control experiments are also shown on Figure 2. In mice injected with a 100-fold excess of unlabeled trastuzumab (n = 3), tumor localization was less apparent. In tumor-free mice (n = 3), the radioactivity distribution over time was similar to that of the tumor-bearing mice with the exception that the dominant signal intensity arose from activity in the circulation; accumulation at sites that would typically contain tumor nodules was not evident. The distribution pattern seen with the irrelevant, anti-CD33 mAb (n = 6) was similarly dominated by activity in the circulation.

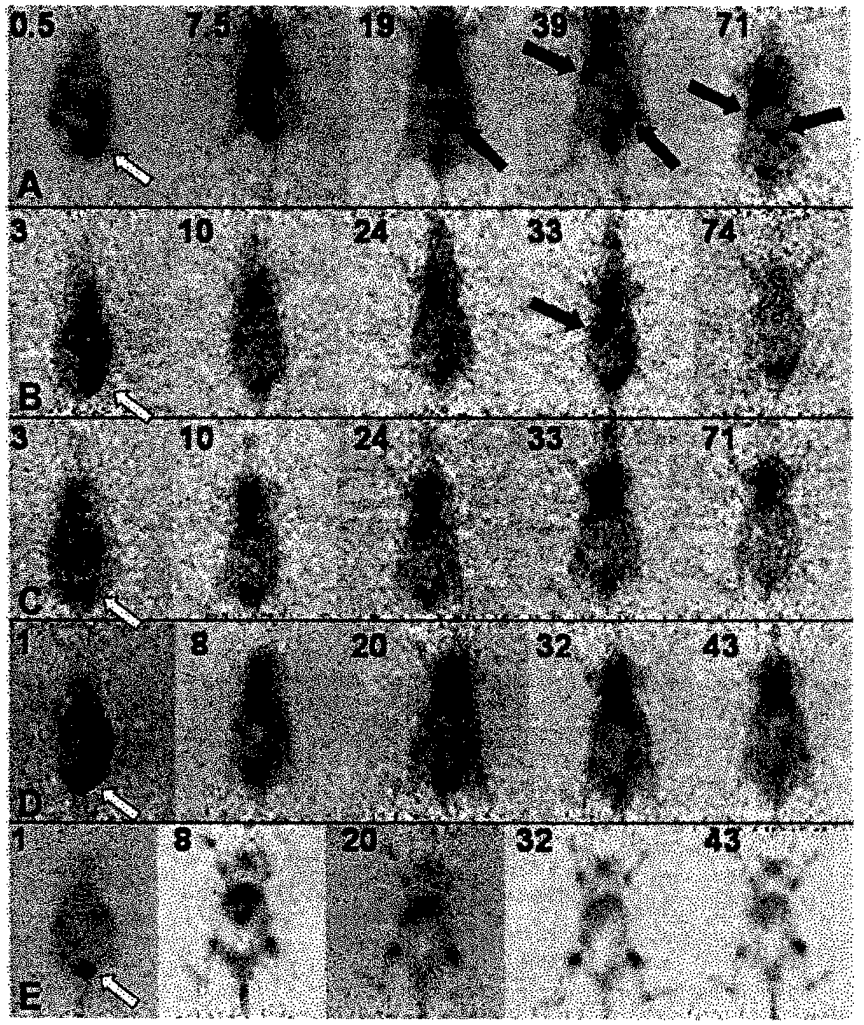

FIGURE 2. Longitudinal microPET coronal slice images of ^{86}Y-trastuzumab (A), excess unlabeled trastuzumab (B), ^{86}Y-trastuzumab on nontumor-bearing mice (C), ^{86}Y-HuM195 (D), and free ^{86}Y (E). Numbers in upper left corner of each panel indicate time after injection (in hours). Black arrows indicate mAb accumulation at confirmed tumor sites. White arrows indicate injection site.

Images obtained after the administration of free ^{86}Y (likely to be ^{86}Y-phosphate on injection; $n = 4$) showed, as expected, accumulation in bone. The whole skeleton was visualized in these studies, with a slightly higher uptake around the various joints. These studies were useful in ensuring that the pattern observed with the specific mAb was due to radiolabeled mAb localization rather than localization of free ^{86}Y, as might arise because of degradation of the chelated mAb. Such a pattern was only observed to a small extent, at 43 h after injection for the irrelevant control studies.

MRI

Figure 3, illustrates the typical tumor distribution observed in our model. In Fig. 3A, high-resolution transverse MR image slices obtained at 1.5 T are registered to corresponding micro-PET slices, providing anatomic context regarding the location of tumor nodules. The images in Fig. 3B depict multiple small (<1-mm diameter) tumor nodules associated with the spleen (left panel) and the mesentery (right panel).

Pharmacokinetics

Whole-body clearance was determined from the total counts in each image set. The specific mAb had the slowest clearance ($t_{1/2} = 160 \pm 10$ h [mean ± SE]), but not significantly different from that of the irrelevant HuM195 ($t_{1/2} = 150 \pm 50$ h) or free ^{86}Y ($t_{1/2} = 140 \pm 50$ h). Controls with an excess of unlabeled specific mAb had a more rapid whole-body clearance ($t_{1/2} = 90 \pm 20$ h), similar to that of specific mAb in nontumor-bearing mice ($t_{1/2} = 110 \pm 60$ h).

The group of mice receiving the specific mAb was evaluated for tumor and organ dosimetry. Initially, the activity concentration over the injection site decreased rapidly, reflecting redistribution in the circulation. This was followed by a slow uptake to a plateau level due to tumor at the trocar wound site (Fig. 4A). Blood kinetics showed a rapid uptake phase, followed by a slow clearance. Tumor had an essentially instantaneous uptake, slowly increasing to the stable maximum activity concentration at around 40 h after injection (Fig. 4B).

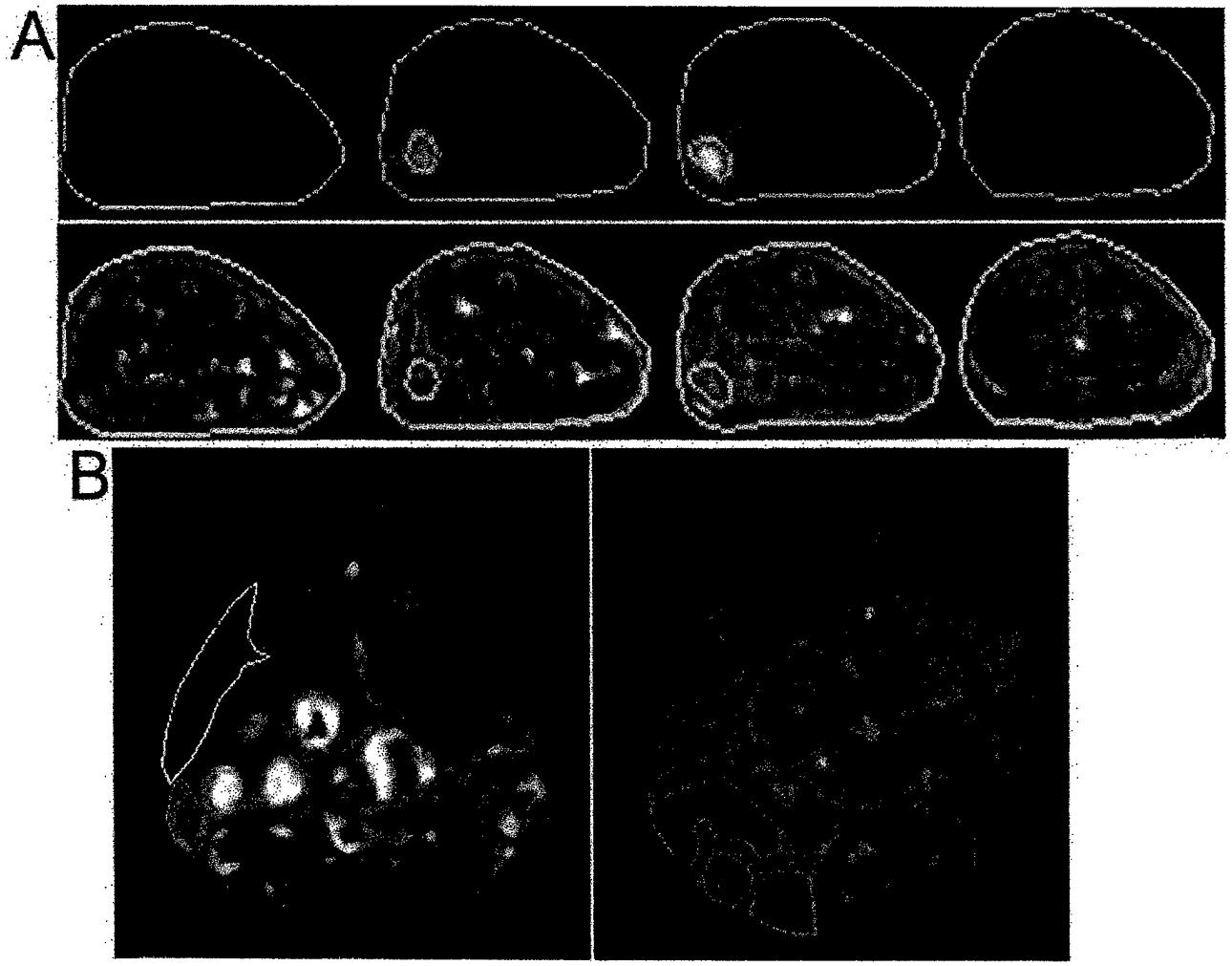

FIGURE 3. (A) High-resolution transverse MR image slices, registered to corresponding microPET slices. Contours depicting outer periphery of mouse and also collection of tumor nodules near spleen are shown. (B) Two transverse MR slices, obtained on small-animal (4.7 T) scanner, are shown. Two slices are taken at different transaxial positions. Slice on left is through spleen (yellow contour), kidneys (blue), and tumor nodules (orange). Slice on right is posterior to left slice and depicts multiple small tumor nodules in mesentery.

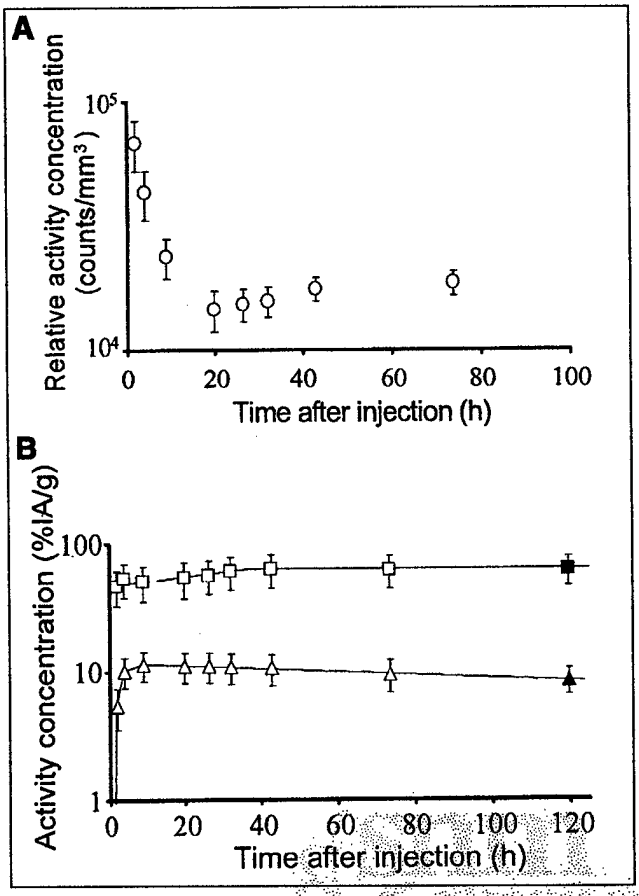

FIGURE 4. (A) Time–activity curve over injection site. Relative activity concentrations were determined by drawing ROIs on microPET image sets. Data are corrected for acquisition time, physical decay, and background. Error bars represent SE. (B) Time–activity curves for blood (triangles) and tumor (squares). Open symbols represent relative activity concentration (e.g., pharmacokinetics) derived from repeated microPET imaging. Activity concentrations (%IA/g) in dissected tissue (solid symbols) were used to quantitate image-based relative concentrations. Error bars represent combined standard uncertainty. Lines show fits used for cumulated activity calculations.

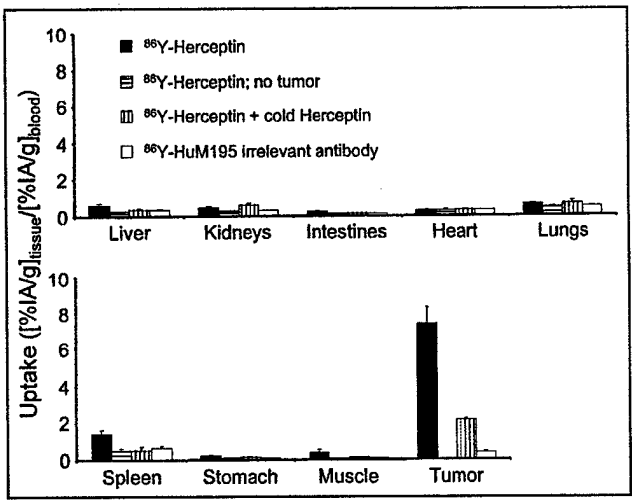

FIGURE 5. Uptake in various tissues 6 d after intraperitoneal injection with ^{86}Y-trastuzumab (^{86}Y-Herceptin), excess unlabeled (cold) trastuzumab, and ^{86}Y-HuM195. Mean values and SE are shown.

Biodistribution

The radioactivity distribution, obtained by well scintillation (γ) counting of excised tissues is shown in Figure 5. Uptake was represented as the organ-to-blood activity concentration ratio. The highest uptake, 7.4 ± 0.9 (mean ± SE), was found for ^{86}Y-trastuzumab specific mAb on tumor. When a 100-fold excess of unlabeled trastuzumab mAb was added, the uptake in tumor was reduced to 2.2 ± 0.1. With the irrelevant, anti-CD33 mAb the uptake was 0.4 ± 0.1.

Spleen had the second highest uptake for the specific mAb with an activity concentration 1.4 ± 0.2 greater than that of blood. The irrelevant mAb gave a slightly lower value of 0.7 ± 0.1. The increased specific uptake may be due to the accumulation of mAb in sites of occult disease within the spleen. Organ-to-blood activity concentration ratios for free ^{86}Y approached infinity due to the exceedingly low radioactivity concentration in blood.

Dosimetry

Absorbed dose to tumor and select organs was calculated for mice receiving ^{90}Y-trastuzumab. Activity concentrations determined from γ-counting dissected tissue was used to scale the ROI contents of the microPET images. The absorbed dose to the kidneys was 0.31 Gy/MBq ^{90}Y-trastuzumab. The liver received 0.48 Gy/MBq, and the spleen received 0.56 Gy/MBq. Because tumors varied in size, calculations were made for spheres of various radii. ^{90}Y activity was assumed to be uniformly distributed throughout the spheres. Absorbed dose to tumors varied from 0.10 Gy/MBq for radius = 0.1 mm to 3.7 Gy/MBq for radius = 5 mm. Results are summarized in Table 1.

DISCUSSION

There is now a preponderance of evidence to suggest that radioimmunotherapy will be most successful in the treatment

TABLE 1
Absorbed Doses to Organs and Tumors of Varying Sizes After Intraperitoneal Injection of ^{90}Y-Trastuzumab

Organ or tumor	Radius (mm)	Absorbed fraction	Dose (Gy/MBq)
Tumor	0.1	0.017	0.10
Tumor	0.5	0.084	0.48
Tumor	1.0	0.17	0.96
Tumor	3.0	0.45	2.6
Tumor	5.0	0.63	3.7
Liver		0.69	0.48
Kidneys		0.52	0.31
Spleen		0.34	0.56

Calculation based on pharmacokinetics and biodistribution of intraperitoneally injected ^{86}Y-trastuzumab.

of micrometastatic disease (*22–24*). Most animal models evaluating tumor response rely on tumor volume measurements obtained by external, caliper-based measurements. Because this approach is not amenable to the evaluation of therapy against micrometastases, the preclinical evaluation of such is usually performed by assessing animal morbidity, secondary to macroscopic growth of the micrometastases (*12*). Using a positron-emitter–labeled mAb and microPET imaging we have demonstrated the ability to image, monitor targeting kinetics, and perform dosimetry of micrometastases at clinically relevant dimensions, noninvasively.

This approach is fundamentally different from studies examining gene expression, in which a reporter gene is cotransfected with the gene sequence to be studied (*25–27*). The ability to visualize disease with this approach is critically dependent on the mAb chosen, accessibility of the tumor cells to the injected mAb, and the degree to which the targeted antigen is expressed on tumor cells. These conditions are analogous to the conditions required for successful imaging in patients.

Relative to other small-animal imaging modalities (e.g., optical and MRI), microPET is characterized by a very high sensitivity but limited resolution. The high sensitivity is of great advantage in the detection of minimal disease over the whole body. Using microPET to identify the sites of metastatic spread and then using MRI to image these sites at high resolution, it is possible to use these 2 modalities in a complementary fashion.

The β-particle emitter, ^{90}Y, is one of the most frequently used radionuclides for targeted radionuclide therapy (*2,28–30*). Recently, the Food and Drug Administration approved use of the ^{90}Y-anti-CD20 mAb (^{90}Y-ibritumomab tiuxetan [Zevalin]; IDEC Pharmaceutical Corp.) for treating various non-Hodgkin's lymphomas (*31*). ^{90}Y does not emit photons that can be used to obtain pharmacokinetics; biodistribution for dosimetry calculations is, therefore, typically obtained by imaging using the surrogate radiometal ^{111}In. Although this radionuclide has been shown to have a generally similar behavior to ^{90}Y, several differences have been noted (*3,4,32*). Using the chemically identical positron emitter, ^{86}Y, the true distribution of the therapeutic radionuclide, ^{90}Y, is used in this work.

The methodology outlined in this work for microPET-based dosimetry overcomes several important limitations in direct microPET quantitation. As noted in the methods, microPET quantitation can be influenced by the position of tissue relative to the central axis of the camera and also by the tissue surrounding the ROI. In imaging micrometastases, wherein the activity containing volume is below the intrinsic resolution of the camera, partial-volume effects also become important. These concerns were addressed by relating the time course of PET measurements to γ-counting results and by maintaining ROIs that were greater than the apparent intensity volume.

CONCLUSION

For all injected compounds, the relative microPET image intensity of the tumor matched the subsequently determined ^{86}Y uptake. Coregistration with MR images confirmed the position of ^{86}Y uptake relative to various organs. Radiolabeled trastuzumab mAb was shown to localize to sites of disease with minimal normal organ uptake. Dosimetry calculations showed a strong dependence on tumor size. These results demonstrate the usefulness of combined microPET and MRI for the evaluation of novel therapeutics.

ACKNOWLEDGMENTS

We thank Virginia Pellegrini, BS, for providing excellent assistance with cell culture. This work was supported, in part, by National Institutes of Health/National Cancer Institute grants CA-08748, 1R24CA83084, R24CA83084, R01CA62444, and P01CA86438; by U.S. Army grant DAMD17-00-1-0429; by Department of Energy grant DE-FG02-86ER-60407; and by a Swedish Cancer Society Fellowship.

REFERENCES

1. Gordon LI, Witzig TE, Wiseman GA, et al. Yttrium-90 ibritumomab tiuxetan radioimmunotherapy for relapsed or refractory low-grade non-Hodgkin's lymphoma. *Semin Oncol.* 2002;29(suppl):87–92.
2. Wiseman GA, White CA, Sparks RB, et al. Biodistribution and dosimetry results from a phase III prospectively randomized controlled trial of Zevalin radioimmunotherapy for low-grade, follicular, or transformed B-cell non-Hodgkin's lymphoma. *Crit Rev Oncol Hematol.* 2001;39:181–194.
3. Lövqvist A, Humm JL, Sheikh A, et al. PET imaging of ^{86}Y-labeled anti-Lewis Y monoclonal antibodies in a nude mouse model: comparison between ^{86}Y and ^{111}In radiolabels. *J Nucl Med.* 2001;42:1281–1287.
4. Garnestani K, Milenic DE, Plascjak PS, Brechbiel MW. A new and convenient method for purification of ^{86}Y using a Sr(II) selective resin and comparison of biodistribution of ^{86}Y and ^{111}In labeled Herceptin. *Nucl Med Biol.* 2002;29:599–606.
5. Leyland-Jones B. Trastuzumab: hopes and realities. *Lancet Oncol.* 2002;3:137–144.
6. Zinner RG, Kim J, Herbst RS. Non-small cell lung cancer clinical trials with trastuzumab: their foundation and preliminary results. *Lung Cancer.* 2002;37:17–27.
7. Baselga J, Norton L, Albanell J, Kim YM, Mendelsohn J. Recombinant humanized anti-HER2 antibody (Herceptin) enhances the antitumor activity of paclitaxel and doxorubicin against HER2/neu overexpressing human breast cancer xenografts. *Cancer Res.* 1998;58:2825–2831.
8. Bunn PA Jr, Helfrich B, Soriano AF, et al. Expression of Her-2/neu in human lung cancer cell lines by immunohistochemistry and fluorescence in situ hybridization and its relationship to in vitro cytotoxicity by trastuzumab and chemotherapeutic agents. *Clin Cancer Res.* 2001;7:3239–3250.
9. Kotts CE, Su FM, Leddy C, et al. ^{186}Re-Labeled antibodies to p185HER2 as HER2-targeted radioimmunopharmaceutical agents: comparison of physical and biological characteristics with ^{125}I and ^{131}I-labeled counterparts. *Cancer Biother Radiopharm.* 1996;11:133–144.
10. Mujoo K, Maneval DC, Anderson SC, Gutterman JU. Adenoviral-mediated p53 tumor suppressor gene therapy of human ovarian carcinoma. *Oncogene.* 1996;12:1617–1623.
11. Borchardt P, Quadri SM, Freedman RS, Vriesendorp HM. Intraperitoneal radioimmunotherapy with human monoclonal IGM in nude mice with peritoneal carcinomatosis. *Cancer Biother Radiopharm.* 2000;15:53–64.
12. McDevitt MR, Ma D, Lai LT, et al. Tumor therapy with targeted atomic nanogenerators. *Science.* 2001;294:1537–1540.
13. Finn RD, McDevitt M, Ma D, et al. Low energy cyclotron production and separation of yttrium-86 for evaluation of monoclonal antibody pharmacokinetics and dosimetry. In: Duggan JL, Morgan IL, eds. *Applications of Accelerators in Research and Industry: Proceedings of the Fifteenth International Conference.* Woodbury, NY: American Institute of Physics Press; 1999:991–993.

14. Nikula TK, Curcio MJ, Brechbiel MW, Gansow OA, Finn RD, Scheinberg DA. A rapid, single vessel method for preparation of clinical grade ligand conjugated monoclonal antibodies. *Nucl Med Biol.* 1995;22:387–390.
15. Nikula TK, McDevitt MR, Finn RD, et al. Alpha-emitting bismuth cyclohexylbenzyl DTPA constructs of recombinant humanized anti-CD33 antibodies: pharmacokinetics, bioactivity, toxicity and chemistry. *J Nucl Med.* 1999;40:166–176.
16. Xu S, Gade TPF, Matei C, et al. In vivo multiple-mouse imaging at 1.5T. *Magn Reson Med.* 2003;49:551–557.
17. Kolbert KS, Hamacher KA, Jurcic JG, Scheinberg DA, Larson SM, Sgouros G. Parametric images of antibody pharmacokinetics in Bi213-HuM195 therapy of leukemia. *J Nucl Med.* 2001;42:27–32.
18. Kolbert KS, Sgouros G, Scott AM, et al. Implementation and evaluation of patient-specific three-dimensional internal dosimetry. *J Nucl Med.* 1997;38:301–308.
19. Loevinger R, Budinger T, Watson E. *MIRD Primer For Absorbed Dose Calculations.* New York, NY: Society of Nuclear Medicine; 1988:1–17.
20. Bardies M, Chatal JF. Absorbed doses for internal radiotherapy from 22 beta-emitting radionuclides: beta dosimetry of small spheres. *Phys Med Biol.* 1994; 39:961–981.
21. Kolbert KS, Watson T, Matei C, Xu S, Koutcher JA, Sgouros G. Murine S factors for liver, spleen, and kidney. *J Nucl Med.* 2003;44:784–791.
22. Goldenberg DM. Targeted therapy of cancer with radiolabeled antibodies. *J Nucl Med.* 2002;43:693–713.
23. DeNardo SJ, Williams LE, Leigh BR, Wahl RL. Choosing an optimal radioimmunotherapy dose for clinical response. *Cancer.* 2002;94(suppl):1275–1286.
24. Mattes MJ. Radionuclide-antibody conjugates for single-cell cytotoxicity. *Cancer.* 2002;94(suppl):1215–1223.
25. Jacobs A, Tjuvajev JG, Dubrovin M, et al. Positron emission tomography-based imaging of transgene expression mediated by replication-conditional, oncolytic herpes simplex virus type 1 mutant vectors in vivo. *Cancer Res.* 2001;61:2983–2995.
26. Doubrovin M, Ponomarev V, Beresten T, et al. Imaging transcriptional regulation of p53-dependent genes with positron emission tomography in vivo. *Proc Natl Acad Sci USA.* 2001;98:9300–9305.
27. Gambhir SS, Herschman HR, Cherry SR, et al. Imaging transgene expression with radionuclide imaging technologies. *Neoplasia.* 2000;2:118–138.
28. Waldherr C, Pless M, Maecke HR, Haldemann A, Mueller-Brand J. The clinical value of [^{90}Y-DOTA]-D-Phe1-Tyr3-octreotide (^{90}Y-DOTATOC) in the treatment of neuroendocrine tumours: a clinical phase II study. *Ann Oncol.* 2001;12:941–945.
29. Paganelli G, Zoboli S, Cremonesi M, et al. Receptor-mediated radiotherapy with ^{90}Y-DOTA-D-Phe1-Tyr3-octreotide. *Eur J Nucl Med.* 2001;28:426–434.
30. Richman CM, DeNardo SJ. Systemic radiotherapy in metastatic breast cancer using ^{90}Y-linked monoclonal MUC-1 antibodies. *Crit Rev Oncol Hematol.* 2001; 38:25–35.
31. Crawford LM Jr. From the Food and Drug Administration. *JAMA.* 2002;287: 1640.
32. Clarke K, Lee F-T, Brechbiel MW, Smyth FE, Old LJ, Scott AM. In vivo biodistribution of a humanized anti-Lewis Y monoclonal antibody (hu3S193) in MCF-7 xenografted BALB/c nude mice. *Cancer Res.* 2000;60:4804–4811.

Alpha-particle emitting atomic generator (Ac^{225})-labeled Herceptin targeting breast cancer spheroids: efficacy versus HER-2/*neu* expression

Åse M Ballangrud, Wei-Hong Yang, Stig Palm, Richard Enmon, Paul E Borchardt, Virginia A Pellegrini, Michael R McDevitt, David A Scheinberg, George Sgouros

Abstract

The humanized monoclonal antibody, Herceptin (trastuzumab), directed against HER-2/*neu*, has, been effective in the treatment of breast cancer malignancies overexpressing HER-2/*neu* in combination with chemotherapy. Radiolabeled Herceptin has been previously considered as a potential agent for radioimmunotherapy. The objective of this study was to investigate the efficacy of Herceptin labeled with the alpha-particle emitting atomic generator, actinium-225 (^{225}Ac), against breast cancer spheroids with different HER-2/*neu* expression levels. ^{225}Ac has a 10 day half-life and a decay scheme yielding 4 alpha-particles, with initial energies in the range 5-8 MeV. The breast carcinoma cell lines MCF7, MDA-MB-361 (MDA) and BT-474 (BT) with relative HER-2/*neu* expression (by FACS) of 1:4:18 were used. Spheroids of these cell lines were incubated with different concentrations of ^{225}Ac-Herceptin and spheroid growth was measured by light microscopy over a 50-day period. The activity concentration required to yield a 50% reduction in spheroid volume at day 35 was 11.8, 1.1 and 0.4 kBq/ml (320, 30, 10 nCi/ml) for MCF7, MDA and BT spheroids, respectively. MCF7 spheroids continued growing but with a 20 to 30 day growth delay at 18.5 kBq/ml. MDA spheroid growth was delayed by 30 to 40 days at 3.7 kBq/ml; at 18.5 kBq/ml, 12/12 spheroids disaggregated after 70 days and cells remaining from each spheroid failed to form colonies within 2 weeks of being transferred to adherent dishes. Eight of ten BT spheroids failed to regrow at 1.85 kBq/ml. All BT spheroids at activity concentrations >3.7 kBq/ml failed to regrow and to form colonies. The radiosensitivity of these 3 lines as spheroids was evaluated as the activity concentration required to reduce the treated to

untreated spheroid volume ratio to 0.37, DVR_{37}. An external beam radiosensitivity of 2 Gy was found for spheroids of all three cell lines. Following alpha-particle irradiation a DVR_{37} of 1.5, 3.0, and 2.0 kBq/ml was determined for MCF7, MDA, and BT, respectively. The concentrations used in these studies translate to human administered activities in the mCi to sub-mCi range. These studies suggest that ^{225}Ac labeled Herceptin may be a potent therapeutic agent against metastatic breast cancer cells exhibiting a wide range of HER-2/*neu* expression.

Introduction

The humanized monoclonal antibody, Herceptin, directed against HER-2/*neu*, has in combination with chemotherapy, been effective in the treatment of breast cancer malignancies overexpressing HER-2/*neu* (1-4). This work examines a treatment approach using Herceptin labeled with the alpha particle emitting atomic generator, actinium-225, to eradicate breast cancer metastases expressing variable levels of HER-2/*neu*.

The HER-2/*neu* oncogene encodes a transmembrane protein ($p185^{HER2}$) with extensive homology to the epidermal growth factor (EGF) receptor. Amplification and overexpression of HER-2/*neu* have been documented in many human tumors, most notably in breast cancer (17-18). The expression of HER-2/*neu* is relatively stable over time and is generally congruent at different metastatic sites (17, 21). However, HER-

2/*neu* protein has also been identified on cell membranes of epithelial cells in the gastro-intestinal, respiratory, reproductive, and urinary tract as well as in the skin, breast and placenta. HER-2/*neu* expression levels in these normal tissues are similar to the levels found in non-amplified, non-overexpressing breast cancers cells (18). Approximately 30% of breast cancer patients have tumors overexpressing the HER-2/*neu* receptor. Herceptin treatment has been limited to these patients because of the cross-reactivity with normal tissues noted above. HER-2/*neu* has been previously considered for radioimmunotherapy against breast cancer. The beta emitter, I-131 (23), and also Pb-212 (24), whose daughter, Bi-212, decays by alpha particle emission, have been labeled to antibodies targeting HER-2/*neu* and investigated in animal models.

The alpha-particle emitting atomic generator, ^{225}Ac, has a 10-day half-life and each decay of ^{225}Ac leads to the emission of four alpha particles (Fig. 1), greatly increasing its efficacy over previously considered alpha-particle emitters (*13*). Studies, *in vitro*, and in animal models have shown that this radionuclide is approximately 1000-fold more effective per unit radioactivity than ^{213}Bi, a first generation alpha-emitter that is currently under clinical investigation (Sgouros, jurcic blood 2002). Studies in animals, however, have also shown that, depending upon the administration route, target and chelation chemistry, it is also substantially more toxic (McDevitt Science, Kennel). The increased efficacy arises because ^{225}Ac has a longer half-life (10 days vs. 45.6 min for ^{213}Bi), increasing the total number of decays per unit radioactivity and allowing prolonged irradiation of targeted cells and also because its decay leads to the release of 3 alpha-particle emitting daughters. The toxicity arises because chelate conjugated antibody

delivery of this radionuclide can only retain, within the chelate, the first of the four alpha emitting atoms. The chelation of the radionuclide is disrupted upon transformation of the parent atom and emission of the first alpha; subsequent alpha-emitting daughter atoms are, therefore, free to possibly distribute elsewhere in the body and potentially irradiate normal organs (). This will be mitigated if the radiolabeled antibody is internalized since charged daughter atoms produced intracellularly are retained within the cell (Science paper).

Herceptin mediated targeting of ^{225}Ac to disseminated breast cancer, therefore, will be a viable therapeutic approach in humans only if the two fundamental problems outlined above are addressed. First the high background expression of HER-2/*neu* in normal tissues must be obviated, as this cross-reactivity is likely to lead to alpha-particle irradiation of normal tissues. Second, the potential toxicity associated with the distribution of free, alpha-particle emitting daughters, resulting from the decay of ^{225}Ac must be overcome. Both of these requirements may be met by targeting rapidly accessible micrometastatic disease in a treatment schedule in which intravenously administered ^{225}Ac-Herceptin is allowed to distribute for several hours and is then cleared from the circulation, either by direct physical means such as extracorporeal immunoadsorption () or by administration of secondary clearing agents (). Extravasation of intact antibody into normal tissue parenchyma generally requires 24 to 48 hours (). By rapidly decreasing the concentration of circulating antibody, binding to normal cross-reactive tissues would be reduced substantially, while also reducing the ^{225}Ac

concentration in the circulation and, therefore, the subsequent concentrations of free daughters.

Such a treatment strategy has been investigated, *in vitro*, using the spheroid model to represent rapidly accessible, intravascularly distributed tumor cell clusters. In anticipation of variable HER-2/*neu* expression in a particular population of breast carcinoma cells, efficacy against cells with different HER-2/*neu* expression levels has been examined. In contrast to traditional radioimmunotherapy with beta-particle emitters which kill cells over a large, multi-mm, range, alpha particles can kill individual cells; therefore antigen density on the target cell will play an accordingly greater role in efficacy.

Materials and methods

Cells

The breast carcinoma cell lines, MCF7, MDA-MB-361 (MDA) and BT-474 (BT) were purchased from the American Type Culture Collection (ATCC, Manassas, VA). MCF7 monolayer cultures were incubated in MEM with NEAA (MSKCC Media Lab, NY), MDA in L-15 (MSKCC Media Lab, NY), and BT in RPMI with 10mM HEPES, 1mM NA Pyruvate, 2mM L-Glutamine, 1.5g/L Bicarbonate, and 4.5g/L Glucose (MSKCC Media Lab, NY). The medium for all cell lines was supplemented with 10% FBS, 100 units/ml penicillin, and 100 µg/ml streptomycin. The cell cultures were kept at 37°C in a humidified 5% CO_2 and 95% air incubator.

Spheroids

Spheroids were initiated using the liquid overlay technique of Yuhas et al. (17, 33). Approximately 10^6 cells, obtained by trypsinization from growing monolayer cultures, were seeded into 100 mm dishes coated with a thin layer of 1% agar (Bacto Agar, Difco, Detroit, MI) with 15 ml of medium. The medium used was the same as for monolayer cultures. After 5 to 7 days, spheroids with approximate diameters of 200±20 μm were selected under an inverted phase-contrast microscope with an ocular scale using an Eppendorf pipette. The selected spheroids were transferred to 35 mm bacteriological petri dishes in 2 ml medium for treatment.

Spheroids selected for disaggregation were centrifuged at 100g for 1 min to remove medium. The pellet was then suspended and gently mixed in pre-heated (37 °C) PBS containing 0.25 % trypsin and 1 m*M* EDTA. Light microscopy was used to monitor the mixture for spheroid dissociation and membrane blebbing as an early indicator of membrane rupture. Dissociation normally occurred within 2 minutes, during which blebbing of cells was minimal. The suspension was immediately centrifuged at 75g for 45 s to remove trypsin and the pellet re-suspended in PBS for flow cytometry.

Flow Cytometry

The relative level of HER-2/*neu* expression for the three cell lines was determined using the Becton-Dickinson FACS Caliber Analyzer (Franklin Lakes, NJ). HER-2/*neu* expression was determined for cells from monolayer culture and cells from disaggregated

spheroids. The cells were first incubated with Herceptin for 0.5 hours, then washed and incubated (0.5 h) with a fluorescently tagged antibody against the F_c portion of human IgG (Sigma, F-9512). A total of 10,000 events were collected.

Antibodies

Herceptin (anti-HER-2/*nue*) (Genentech, Inc., South San Francisco, CA) was used as the specific antibody. HuM195 (anti-CD33) (Protein Design Laboratories, Inc. Sunnyview, CA) and J591 (anti-PSMA) (generously supplied by Dr. Neil Bander, Department of Urology, New York Presbyterian Hospital-Weill Medical College of Cornell University and Ludwig Institute for Cancer Research, New York, NY) were used as non-specific controls.

Confocal Microscopy

Spheroids of diameter 200 μm were incubated with 10 μg/ml FITC- (F7250, Sigma, St. Louis, MO.) conjugated Herceptin for 1, 3 and 5 h and imaged by confocal microscope (Zeiss LSM 510, Carl Zeiss, Inc. Oberkochen, Germany) while still in the incubation medium. A 3 μm thick optical section was acquired at the center of each spheroid. Five spheroids were imaged for each time point. Antibody concentration as a function of radial distance was obtained using MIAU, a software package developed in-house (46). The method has been previously described (ref CR). Briefly, an erosion element is used to follow the exterior contour of each spheroid and the average pixel intensity in each ring is converted to antibody concentration by calibration with the known external concentration of antibody. The antibody concentration as a function of distance from the

rim of the spheroid was corrected for light attenuation as described previously (CR paper).

^{225}Ac

^{225}Ac was obtained from the Department of Energy (Oak Ridge National Laboratory, Oak Ridge, TN) and was supplied as a dried nitrate residue. The ^{225}Ac activity was measured with a Squibb CRC-17 Radioisotope Calibrator (E.R. Squibb and Sons, Inc., Princeton, NJ) set at 775 and multiplying the displayed activity value by 5. The ^{225}Ac nitrate residue was dissolved in 0.1 mL of 0.2 M Optima grade HCl (Fisher Scientific, Pittsburgh, PA). Metal-free water (MFW) used for this and all other solutions was obtained from a Purelab Plus system (U.S. Filter Corp., Lowell, MA) and was sterile filtered.

Radiolabeling Details regarding the radiolabeling methodology are described in reference (Ref: McDevitt et al. Applied Radiation and Isotopes, 2002).

The first step in construct preparation was the ^{225}Ac-DOTA-NCS chelation reaction. The bifunctional isothiocyanoato-derived 2B-DOTA, 2-(*p*-isothiocyanatobenzyl)-1,4,7,10-tetraazacyclododecane-1,4,7,10-tetraacetic acid was obtained from Macrocyclics (Dallas, TX). Actinium-225 dissolved in 0.2 M HCl was mixed with 200 to 500 mg of 10 g/L DOTA-NCS in MFW, 0.015-0.020 mL of 150 g/L stock *l*-ascorbic acid, and 0.025-0.150 mL of 2 M TMAA (Tetramethylammonium acetate). The mixture was then heated to 60°C for 30-45 min.

The second step in construct preparation was the ^{225}Ac-DOTA-NCS reaction with the IgG. The ^{225}Ac-DOTA-NCS chelation reaction was mixed with 0.5 to 1.0 mg of the IgG, 0.015-0.020 mL of 150 g/L stock *l*- ascorbic acid, and 0.025-0.150 mL of a 1 M carbonate buffer. The reaction mixture was then heated to 36°C for 30 to 60 min. At the end of the reaction period, the mixture was treated with a 0.020 mL addition of 10 mM DTPA (diethylenetriaminepentaacetic acid) to complex any free metals during the size exclusion chromatographic purification using a 10 DG size exclusion column with a 1% HSA as the mobile phase.

The radiochemical purity of ^{225}Ac-DOTA-Herceptin was >90% as determined by instant thin layer chromatography methods and the immunoreactivity of the labeled product was between 70 and 80% as determined by cell based-assay methods (Ref: Nikula et al. J. Nucl. Med. 1999, 40, 166.).

Radiosensitivity

The radiosensitivity of the different cell lines was determined in monolayer cultures using the colony forming assay (ref7). Depending on the radiation dose, between 10^3 and 10^7 cells were plated in monolayer cultures. External beam radiosensitivity was determined following exposure to acute doses of 3, 6, 9, or 12 Gy photon irradiation using a cesium irradiator at a dose rate of 0.8 Gy/min (Cs-137 Model 68, JL Shepherd and Associates, Glendale, CA.). The absorbed dose required to yield a 37% survival, (*i.e.,* the D_0 value) was obtained by fitting a monoexponential function to the log-linear portion of the surviving fraction curve. Monolayer cultures incubated with 3.7, 18.5, and 37 kBq/ml

^{225}Ac-labeled non-specific antibody for 24 hr were used to determine alpha-particle radiosensitivity. Over a 24-hr period, 6.7% of the total number of ^{225}Ac atoms will have decayed. Since the longest lived daughter, Bi-213, has a half-life of 45.6 min, all daughters generated during this period will also decay. Assuming, therefore, that each decay of ^{225}Ac deposits the sum of all 4 alpha-particle energies, the mean absorbed dose is estimated to be 1.4, 6.8, and 13.6 Gy for each of the three concentrations, respectively.

The radiosensitivity of spheroids was evaluated as the activity concentration required to reduce the treated to untreated spheroid volume ratio to 0.37. Since this parameter depends upon the day post-therapy, volume ratios from day 20 to day 45 post-therapy were calculated for each spheroid and the median value across this time-period was used. By plotting this volume ratio versus activity concentration and fitting the log-linear portion of the curve to a monoexponential function, a radiosensitivity parameter may be derived from the slope. The inverse of the slope gives the dose that yields a volume ratio of 0.37. This value is denoted DVR_{37}, and it is loosely analogous to the D_0 in colony formation assays.

Treatment Protocol

The response to ^{225}Ac labeled Herceptin was evaluated by incubating spheroids with 0.37, 1.85, 3.70, or 18.50 kBq/ml ^{225}Ac on 10 μg/ml Herceptin (specific antibody) for 1 hour. Spheroids exposed to 18.50 kBq/ml ^{225}Ac on 10 μg/ml irrelevant antibody (radioactive control), 10 μg/ml unlabeled Herceptin (unlabeled antibody control) and untreated spheroids (control) were followed in the same manner. Twenty-four or twelve

spheroids were used in each experiment. After incubation, the spheroids were washed three times by suspension in fresh medium and placed in separate wells of a 24-well plate. The media in each well was replaced and individual spheroid volume measurements were performed twice per week. An inverted phase microscope fitted with an ocular micrometer was used to determine the major and minor diameter d_{max} and d_{min}, respectively, of each spheroid. Spheroid volume was calculated as $V = \pi \cdot d_{max} \cdot d_{min}^2 / 6$. Volume monitoring was stopped once a spheroid diameter exceeded 1 mm or when the spheroid fragmented to individual cells or smaller (2- to 3- cell) clusters. The viability of such fragments was assessed in an outgrowth assay by plating the cell clusters on to adherent dishes, incubating for 2 weeks, and then evaluating for colony formation or outgrowth.

Results

The relative HER-2/*neu* cell-surface expression of MCF7, MDA and BT cells derived from monolayer culture and from disaggregated spheroids is depicted in figure 2. The highest HER-2/*neu* expressing cell line, BT, shows a decrease in the number of HER-2/*neu* sites (relative to MDA) and also a greater variability in cell surface expression in cells derived from spheroids compared to cells from monolayer culture. The relative expression of HER-2/*neu* in cells derived from monolayers is 1:4:18 (MCF7:MDA:BT) ; the corresponding expression ratios for cells derived from spheroids are 1:6:12.

Penetration of Herceptin into spheroids was evaluated by measuring FITC labeled Herceptin by confocal microscopy. Images acquired through the equator of 200 μm diameter spheroids incubated for 1, 3 and 5 hours with 10 μg/ml Herceptin-FITC are shown for MDA and BT spheroids in figure 3. The cells on the spheroid rim are clearly outlined, consistent with antibody localization to cell-surface HER-2/*neu*. Herceptin has penetrated approximately 1, 2 and 3 cell layers after 1, 3 and 5 hours incubation, respectively. FITC intensity was converted to antibody concentration as described in the methods. The results are depicted in figures 4a and 4b. The concentration of antibody at the surface of BT spheroids after 1 hour incubation is greater than twice that of MDA spheroids. After longer incubation durations, the antibody concentration in MDA spheroids at the surface increases whereas it decreases for BT spheroids giving a concentration ratio that approaches one. At 20 μm from the surface, the antibody ratio on MDA vs BT spheroids is 5 after 1 hour of incubation. The antibody concentration at 20 μm increases with increased incubation time for both spheroid systems but slightly more so for the MDA spheroid, giving a ratio close to 2 by 5 hours.

To examine for a possible differential sensitivity to unlabeled Herceptin antibody, spheroids of the three cell lines were incubated for 1 hour in 10, 50, 100 and 500 μg/ml. No impact upon spheroid growth was observed (data not shown).

To discriminate between inherent radiosensitivity of the different cell lines and increased targeting due to the differential expression of HER-2/*neu*, the radiosensitivity of each cell line was determined in monolayer cultures as well as by following spheroid growth after

external beam irradiation and after incubation with ^{225}Ac labeled non-specific antibody. The surviving fraction of cells in monolayer culture is plotted versus mean absorbed dose for photons and alpha particles in figures 5a and 5b, respectively. The dose, D_0, required to yield a surviving fraction of 37% is listed in table 1. MCF7 cells are 2-fold and 2.4-fold more sensitive to external beam radiation than MDA and BT cells, respectively. Although this cell line is also more sensitive to alpha-particle radiation than MDA and BT, the differences in radiosensitivity are less pronounced.

Spheroid response to 3, 6, 9, and 12 Gy external beam irradiation and increasing concentrations of ^{225}Ac labeled non-specific antibody (24 h incubation) is depicted in figure 6. Fifty days after a 12 Gy external dose, outgrowth assays for MCF7 and BT spheroids showed viable cells, whereas no colonies were formed for MDA spheroids. At the two highest concentrations of ^{225}Ac-labeled non-specific radiolabeled antibody, outgrowth assays for MCF7 and MDA spheroids yielded no colonies; for BT the same result was obtained only at the highest radioactivity concentration used. The dose required to reduce the volume ratio of treated to untreated spheroids to 0.37, DVR_{37}, was used as a measure of spheroid radiosensitivity and is listed in table 2. The DVR_{37} results show no difference amongst spheroids of the 3 cell lines in sensitivity to external beam irradiation. Differences in volume response to alpha-particle irradiation are seen, however, with MCF7 almost a factor of 2 more sensitive than MDA.

Median growth curves for MCF7, MDA and BT spheroids incubated 1 hr with 0.37, 1.85, 3.7, and 18.5 kBq/ml ^{225}Ac on 10 μg/ml Herceptin, or 18.5 kBq/ml on non-specific

antibody (radioactive control) are depicted in figure 7. At day 35, the median volume of spheroids treated with 18.5 kBq/ml ^{225}Ac-Herceptin relative to untreated control spheroids was 34%, 0.8% and 0.2% for MCF7, MDA and BT, respectively. The corresponding values for spheroids treated with ^{225}Ac labeled non-specific antibody (radioactive control) were 65%, 58% and 71%, respectively. The ^{225}Ac activity concentration required to yield a 50% reduction in spheroid volume relative to untreated spheroids at day 35 was 11.8, 1.1 and 0.4 kBq/ml (320, 30, 10 nCi/ml) for MCF7, MDA and BT spheroids, respectively. Growth of individual spheroids following 1 hr incubation with increasing concentrations of ^{225}Ac on 10 μg/ml Herceptin are shown in figure 8. The variability in response of individual spheroids was minimal. At an activity concentration of 1.85 kBq/ml 2 of 12 BT spheroids were viable; no colonies were observed at 3.7 and 18.5 kBq/ml for this cell line. Likewise, no colonies were observed for MDA spheroids treated at 18.5 kBq/ml. Figure 8 depicts optical microscope images of MDA spheroids following ^{225}Ac-Herceptin treatment. By 21 days after incubation with 3.7 kBq/ml sloughing of cells may be observed; by 42 days, however, the spheroid appears to have recovered. At 18.5 kBq/ml, however, no such recovery is observed.

Discussion

Current staging criteria for overexpression of HER-2/neu rely on immunohistochemical staining of biopsy samples. The staining is graded on a scale of 0-3+. The scale incorporates consideration of uniformity and intensity of the staining pattern. High expression is considered to occur at a level of 2+. Studies have shown that this is

equivalent to approximately 2-5 gene copies per cell or XX sites per cell. The cell lines used in this work span the range of expression levels seen in breast cancer patients. By conjugating Ac-225 to Herceptin, patients that would otherwise have been considered low expressors can be made candidates for therapy. Our studies have shown that it is possible to also target metastases of patients that are not necessarily high expressors. Furthermore targeting with an alpha-particle emitter provides the opportunity to overcome escape of cells or tumor cell clusters with heterogeneous expression of HER-2/neu.

We have used the spheroid model as a preliminary, *in vitro*, model to examine the feasibility of targeting breast cancer micrometastases using Herceptin labeled with the atomic alpha-particle generator, ^{225}Ac. In particular, the question of efficacy against tumor cell clusters with differential expression of HER-2/neu was examined. The three cell lines considered approximated low (MCF7), intermediate (MDA MB-361) and high (BT-474) Her-2/neu expressing metastases (). The results suggest that a concentration of radiolabeled antibody may be found that targets intermediate and high expressing tumor nodules but not low HER-2/neu expressing breast tumors. The utility of

The confocal microscopy images of Herceptin concentration profiles show a slightly deeper penetration in the BT spheroids than in the MDA spheroids. The Herceptin concentration at the surface of the BT spheroids after 1 hr incubation is found to be a factor 2-3 higher than for the MDA spheroids while the penetration depth into the spheroids were similar. This is in good agreement with the relative HER-2/*neu* expression of 15:4 for BT:MDA. The range of alpha particles is typically 80-100 μm and, therefore, complete penetration of the antibody is not required to deliver radiation to

the spheroid core. The 10 μg/ml Herceptin concentration used in these studies was, therefore, found adequate for spheroid kill experiments.

Herceptin incubation in monolayer cultures is reported to result in increased cell doubling time leading to increased cell dormancy (ref 5). This was not observed in spheroids where we found that a 1-hour incubation with concentrations up to 500 μg/ml Herceptin had no effect on spheroid growth kinetics for the three cell lines tested. The absence of an effect on spheroids as opposed to monolayer cultures is probably the result of incomplete penetration, increased resistance to cytotoxic and growth inhibitory agents of spheroids relative to monolayer cultures (ref 6).

In monolayer cultures, the two HER-2/*nue* positive cell lines MDA and BT are approximately equivalent in photon radiosensitivity, whereas MCF7 is approximately 2-fold more radiosensitive. MCF7 was also the most sensitive line to alpha-particle irradiation, with MDA having the lowest sensitivity to alphas of the three and BT alpha sensitivity falling between the other two cell lines. MCF7, MDA and BT spheroids were found to have similar external beam radiosensitivity. Spheroids were found to have a greater differential sensitivity to alpha particles than to external beam irradiation even though the opposite is true in monolayer cultures. It is important to note that the radiosensitivity parameter defined in this work for spheroids is not a measure of cell sterilization but rather of volume reduction. Volume reduction encompasses a number of biological variables including the rates of cellular sterilization, removal of sterilized cells, and cellular proliferation.

The response of spheroids to ^{225}Ac-Herceptin was found to be highly dependent on HER-2/*neu* expression. It was possible to sterilize spheroids with intermediate HER-2/*neu* expression and to induce a growth delay in low HER-2/*neu* expressing spheroids by increasing the specific activity of the radiolabeled antibody. A very high specificity relative to the radioactive controls was observed. Targeted spheroids are exposed to the atomic alpha-particle generator for a prolonged time period, whereas exposure is limited to one hour in the radioactive control experiments. Longer radioactive control exposure durations such as the 24-hour period used in the radiosensitivity measurements showed volume reductions similar to those obtained with the 1 hour specific antibody incubation. The very high specificity seen with a short exposure time supports the clearing strategy outlined in the introduction.

Conclusion

We have demonstrated the ability to increase the efficacy of Herceptin against clusters of tumors cells expressing intermediate levels of HER-2/*nue* by labeling Herceptin with the alpha-particle emitting atomic generator, ^{225}Ac. These results suggest that an ^{225}Ac concentration in the range 9.25 - 18.5 kBq/ml (250-500 nCi/ml) may be sufficient to eradicate tumor cells with intermediate HER-2/*nue* expression. This translates to approximately 1 to 2 mCi for human administration. Based on animal studies (ref4), this activity concentration may be clinically realistic.

Acknowledgments

The authors thank P. Jan Hendrikx of the MSKCC Flow Cytometry Core Facility for his assistance with the flow cytometry studies.

Table 1. Dose, D_0, required to reduce surviving fraction of cells in monolayer cultures following external beam and alpha-particle irradiation to 37%.

Cell line	External beam D_0 (Gy)	Alpha-particle D_0 (Gy)
MCF7	0.7	0.3
MDA	1.4	0.5
BT	1.7	0.4

Table 2. Dose required to reduce the treated to untreated spheroid volume ratio to 0.37.

Cell line	External beam DVR_{37} (Gy)	Alpha- particle DVR_{37} (kBq/ml)
MCF7	2	1.5
MDA	2	2.8
BT	2	2.3

Figure legends

Figure 1 Simplified decay scheme for ^{225}Ac. The arrows designate decay by alpha-particle emission; the average energy of emitted alpha-particles is shown next to each arrow. The decay of ^{213}Bi Beta decays are omitted from the figure, as is the short-lived daughter of Bi-213.

Figure 2 Confocal microscopy images of spheroids ($\phi\sim$ 200 mm) following 1, 3 and 5 hr incubation with 10 μg/ml Herceptin-FITC. The black or gray regions reflect presence of Herceptin. Individual cells are clearly outlined in the surface layer of MDA and BT spheroids, consistent with cell-surface localization of HER-2/*nue*. At 10 μg/ml Herceptin-FITC, no uptake of Herceptin was observed in MCF7 spheroids.

Figure 3 Herceptin concentration profiles across the spheroid section at equator following 1, 3 and 5 hr incubation with 10 μg/ml Herceptin-FITC are shown for (a) MDA and (b) BT spheroids. Each curve corresponds to the median of 5 individual spheroid measurements.

Figure 4 Surviving fraction of MCF7, MDA and BT cells in monolayer cultures are shown following acute doses of external beam radiation.

Figure 5 Surviving fraction of MCF7, MDA and BT cells in monolayer cultures are shown following 24 hr incubation with 3.7, 18.5 and 37 kBq/ml ^{225}Ac labeled non-specific antibody.

Figure 6 Spheroid response to external beam irradiation and increasing concentrations of ^{225}Ac labeled non-specific antibody.

Figure 7 Median growth curves for spheroids incubated 1 hr with 0.37, 1.85, 3.7, and 18.5 kBq/ml ^{225}Ac on 10 μg/ml Herceptin, or 18. 5 kBq/ml on non-specific antibody (radioactive control).

Figure 8 Growth of individual spheroids following 1 hr incubation with ^{225}Ac-Herceptin.

Figure 9 Microscope images of MDA spheroids 1, 21, 42 and 59 days post treatment.

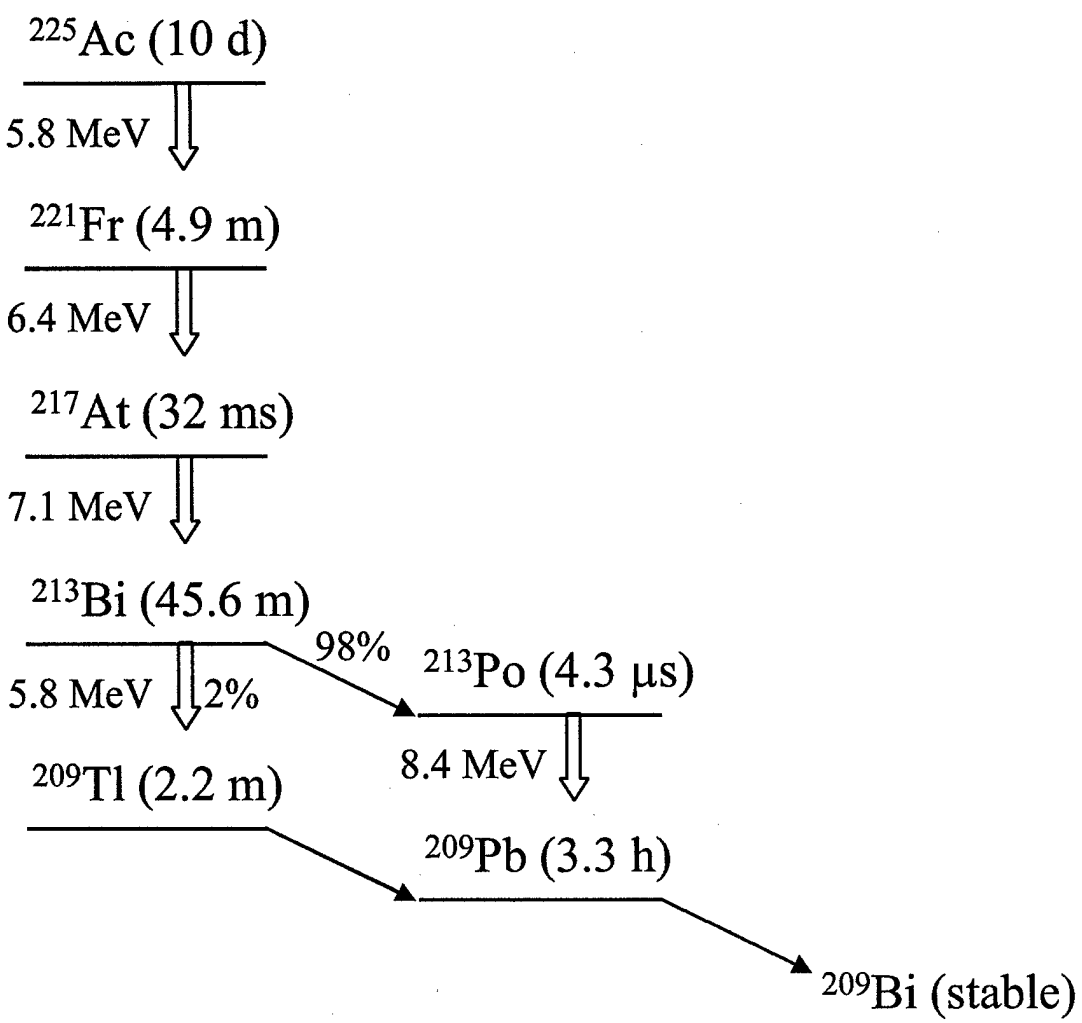
225Ac (10 d)
5.8 MeV
221Fr (4.9 m)
6.4 MeV
217At (32 ms)
7.1 MeV
213Bi (45.6 m)
98%
213Po (4.3 μs)
5.8 MeV
2%
8.4 MeV
209Tl (2.2 m)
209Pb (3.3 h)
209Bi (stable)

Fig. 6

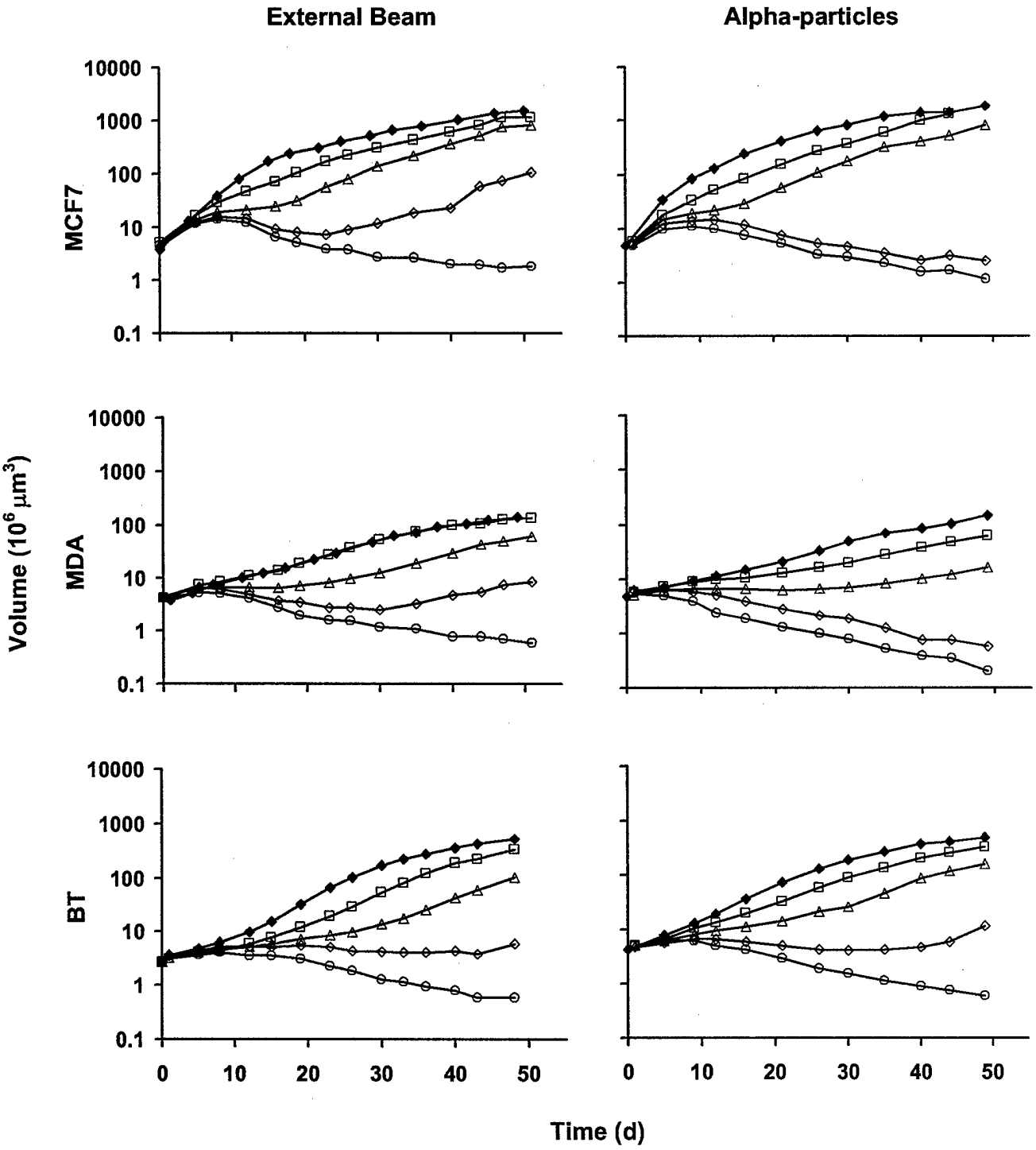
External Beam
Alpha-particles
MCF7
MDA
BT
Volume (10^6 µm^3)
10000
1000
100
10
1
0.1
0
10
20
30
40
50
Time (d)

Fig. 7

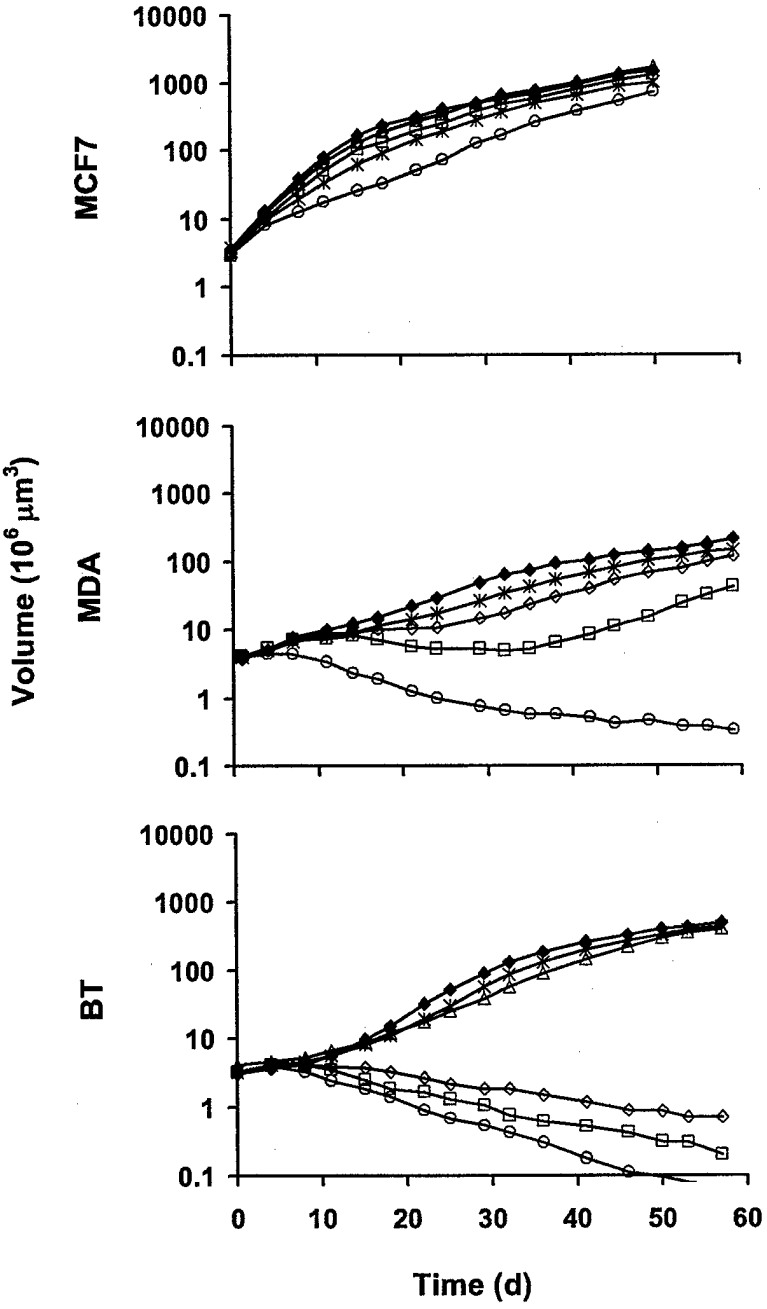
MCF7
MDA
BT
Volume (10^6 µm^3)
10000
1000
100
10
1
0.1
0
10
20
30
40
50
60
Time (d)

Fig. 8

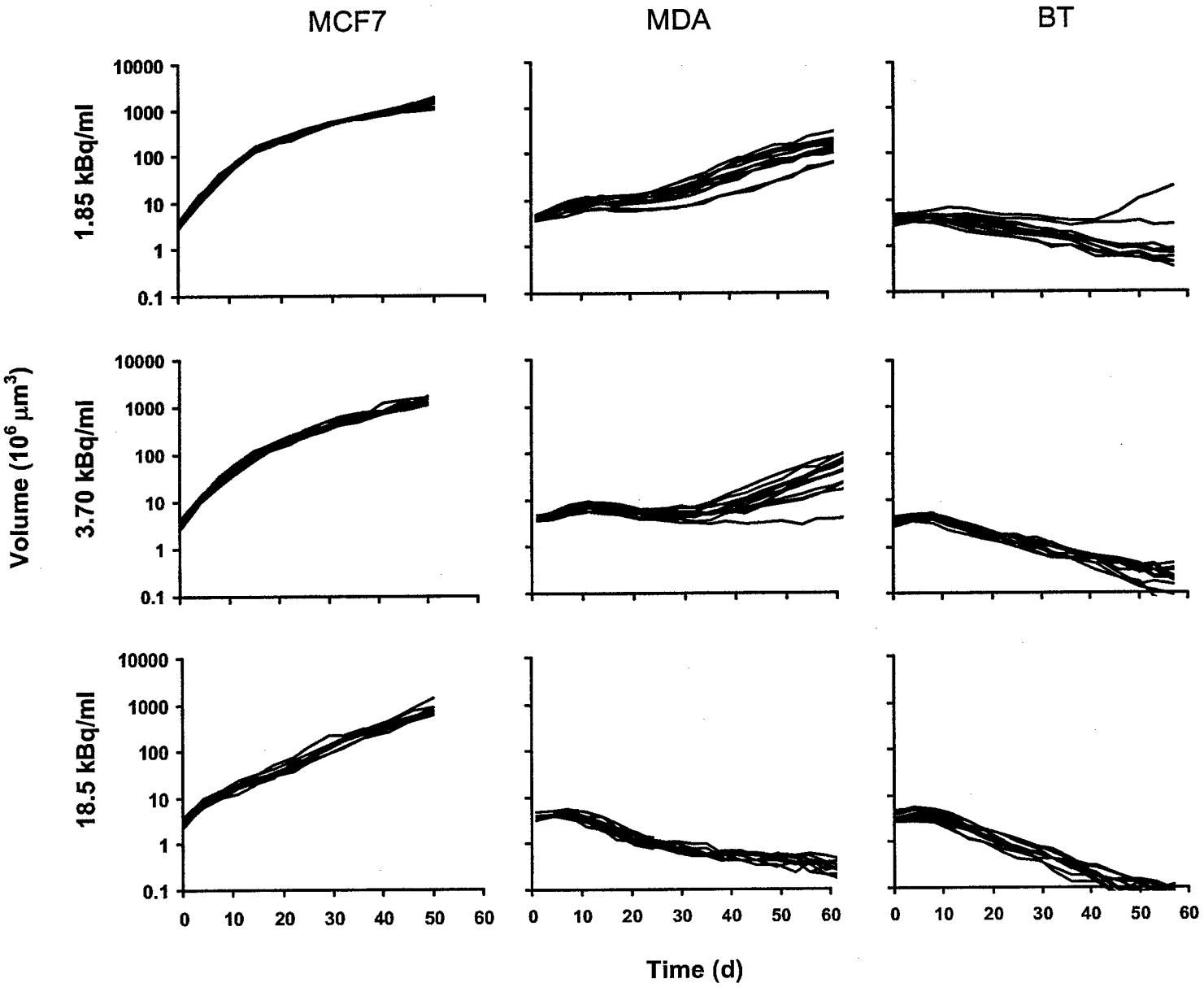
MCF7
MDA
BT
1.85 kBq/ml
3.70 kBq/ml
18.5 kBq/ml
Volume (10^6 µm^3)
10000
1000
100
10
1
0.1
0
10
20
30
40
50
60
Time (d)

Fig. 9

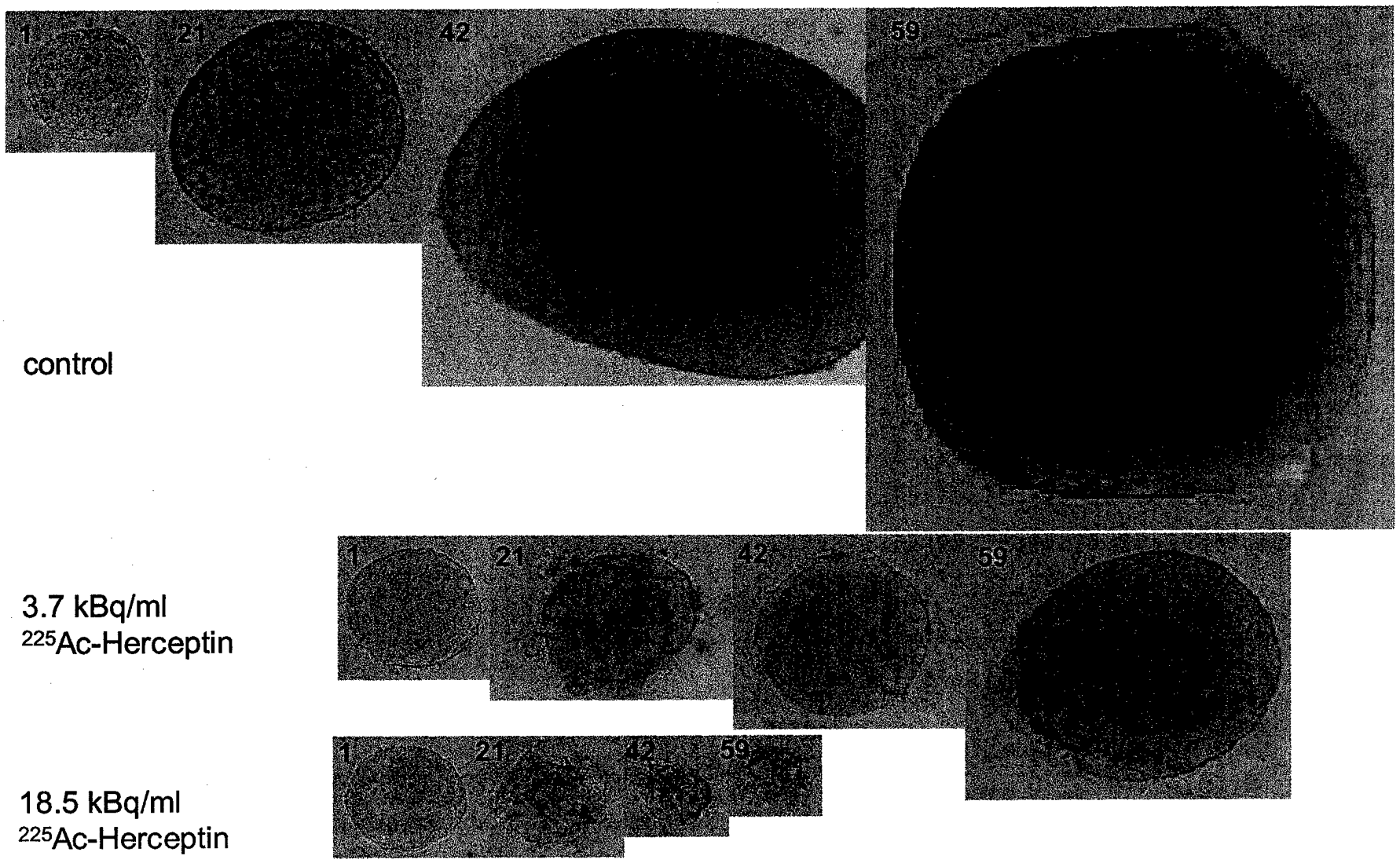
1
21
42
59
control
1
21
42
59
3.7 kBq/ml
225Ac-Herceptin
1
21
42
59
18.5 kBq/ml
225Ac-Herceptin